



Critical assessment of steady-state kinetic models for the synthesis of methanol over an industrial Cu/ZnO/Al₂O₃ catalyst

Y. Slotboom^{a,*}, M.J. Bos^a, J. Pieper^a, V. Vrieswijk^a, B. Likozar^b, S.R.A. Kersten^a, D.W.F. Brilman^{a,*}

^a Sustainable Process Technology, Faculty of Science and Technology, University of Twente, PO Box 217, 7500 AE Enschede, The Netherlands

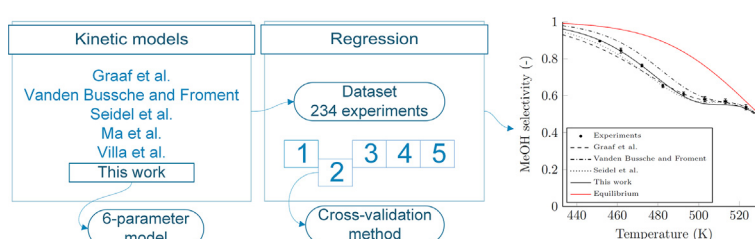
^b Department of Catalysis and Chemical Reaction Engineering, National Institute of Chemistry, Hajdrihova 19, SI-1000 Ljubljana, Slovenia



HIGHLIGHTS

- A novel systematic regression method is developed.
- Available kinetic models are re-fitted and compared on an equal dataset.
- A simple universal and robust kinetic model is presented.

GRAPHICAL ABSTRACT



ARTICLE INFO

Keywords:

Methanol kinetics

CO₂

Syn gas

Cu/ZnO/Al₂O₃

Cross-validation method

ABSTRACT

In this paper a thorough comparison is made between steady state kinetic models for methanol synthesis from Graaf et al. (1988), Vanden Bussche and Froment (1996), Seidel et al. (2018), Ma et al. (2009) and Villa et al. (1985). A new experimental dataset using an industrial Cu/ZnO/Al₂O₃ catalyst is presented and used together with the dataset of Seidel et al. (2018) for refitting the kinetic models. The models are refitted using the statistical cross-validation (CV) method to test for predictive capabilities and model variance. A new kinetic model is proposed with the aim to reduce parameter identifiability problems. The model is derived based on physical observations from literature. This physically consistent model has ten parameters, however more experiments are needed, because the current dataset is not discriminating enough for regression of adsorption isotherms. The proposed model is further reduced to only six parameters. This model is predicting the dataset equally well or better than current higher parameter models. It is shown that the model is a good predicting model for experiments outside the training set. The model is valid for pressures from 20 to 70 bara and temperatures from 450 to 530 K with a high probability of predicting well outside these boundaries.

1. Introduction

Methanol production from renewable resources has become a great interest in research. It is known for its capability of storing renewable energy and most importantly doing this by using CO₂ as a carbon source [1,2]. Methanol can be used in petrol engines, it can be converted to the potential diesel replacement fuel dimethyl ether or it can be used directly in fuel cells [3] to produce electricity. Potentially, it is also a

renewable carbon source for the production of ethylene and propylene by the methanol to olefins (MTO) process as a replacement for fossil oil [2]. Cu-based catalysts have been used for decades in which the industrial Cu/ZnO/Al₂O₃ catalyst has been studied intensively. Over the years there has been debate about the carbon source and the reaction pathway towards methanol. This resulted in a wide range of different kinetic models with varying underlying physical mechanisms. Several methanol production plants using CO₂ have been modeled to predict

* Corresponding author.

E-mail addresses: y.slotboom@utwente.nl (Y. Slotboom), wim.brilman@utwente.nl (D.W.F. Brilman).

<https://doi.org/10.1016/j.cej.2020.124181>

Received 8 October 2019; Received in revised form 20 December 2019; Accepted 20 January 2020

Available online 24 January 2020

1385-8947/ © 2020 The Authors. Published by Elsevier B.V. This is an open access article under the CC BY-NC-ND license (<http://creativecommons.org/licenses/by-nc-nd/4.0/>).

Nomenclature

Symbol Meaning (Unit)

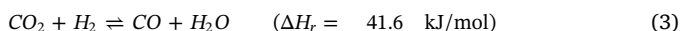
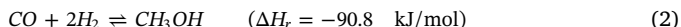
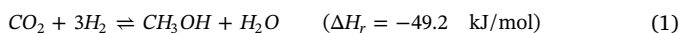
A, B	Arrhenius constants (–)
a, b	Logarithmic Arrhenius constants (–)
A_r	Area of the fixed bed reactor (m^2)
f	Fugacity (bar)
ΔG	Gibbs free energy (J mol^{-1})
ΔH_r	Heat of reaction (kJ mol^{-1})
$K_p^\circ(T)$	Temperature dependent equilibrium constant (–)
k_j	Reaction rate constant (–)
K_i	Adsorption constant (–)
M_{w_i}	Molecular weight (kg mol^{-1})
N	Number of experiments (–)
N_c	Number of components (–)
N_p	Number of parameters (–)
R	Ideal gas constant ($\text{J mol}^{-1}\text{K}^{-1}$)

r_j	Reaction rate ($\text{mol/kg}_{\text{cat}}\text{s}$)
T	Temperature (K)
w_i	Weight fraction (–)
y_i	Mole fraction (–)
\hat{w}_i	Predicted weight fraction (–)
ϵ_b	Fixed bed porosity (–)
γ^*	Relative surface contact free energy (–)
Θ^i	Fraction of free surface centers (–)
θ^i	Fugacity dependent free surface coverage (bar^{-1})
$\nu_{i,j}$	Stoichiometric reaction rate constant (–)
ρ	Density (kg m^{-3})
ϕ	Total amount of relative reduced surface centers (–)
ϕ_m	Mass flow (kg s^{-1})
ϕ_V	Standard volume flow (293 K and $1 \cdot 10^5$ Pa) (mL min^{-1})
γ	Volume flow contraction (–)

the viability of methanol synthesis from CO_2 at a larger scale [4–7]. Next to plant modeling, the most efficient and novel reactor configurations for methanol production are of great interest [8–11]. In such studies the kinetic models of Graaf et al. [19] and Vanden Bussche and Froment [16] are most frequently used, with either one of them being chosen by the authors themselves. Meyer et al. [12] compared the use of the Graaf et al. and Vanden Bussche and Froment kinetic models in a methanol synthesis process by CO_2 hydrogenation. They concluded that outside equilibrium regions the user should be familiar with the differences in the kinetic models and that results can be significantly different. Clearly, there is no consensus in literature about which model should be taken and which one is actually the better one.

1.1. Reaction pathway

The carbon source for methanol, as shown in Eqs. (1) and (2), can either be CO_2 or CO . Historically, the source changed from CO [13] to CO_2 [14–17] and eventually towards both [18–20]. In early kinetic models CO was considered to be the active component. Methanol was produced from synthesis gas and CO_2 was considered a stable component.



Later it was discussed that CO_2 could be a reactant itself and CO_2 hydrogenation terms were incorporated in kinetic models [19,21]. The methanol synthesis kinetic models consist of four categories [22]. The first category (Fig. 1, Type 1) is assumed in the models of Takagawa et al. [23], Graaf et al. [19] and Seidel et al. [20]. Methanol is assumed to be formed from both CO and CO_2 . The reverse water gas shift (RWGS) reaction rate is included (Eq. (3)).

The second group (Fig. 1, Type 2) consists of the methanol formation from CO_2 and CO as assumed by Klier et al., McNeil et al. and Ma et al. [21,24,25]. The two hydrogenation reactions are considered as the key reactions. Thereby, a reaction rate for the RWGS reaction is not taken into account and CO_2 cannot be directly converted to CO . The third group (Fig. 1, Type 3) considers the CO_2 hydrogenation reaction as the main reaction pathway towards methanol and is used by Skrzypek et al., Askgaard et al., Kubota et al. and Vanden Bussche and Froment [14–17]. CO can be produced by the RWGS reaction, but is assumed not to be converted to methanol directly. The last group is the mechanism assumed by Villa et al. [13]. They consider CO as the main carbon source for methanol (Fig. 1, Type 4).

Apart from the developments in different kinetic models, authors

have reported changes of catalyst morphology under different feed gas conditions [26,27]. Another insight is the presence of different active sites for CO and CO_2 hydrogenation. Choi et al. [28] investigated this with catalytic experiments on a Cu/ZnO surface after reduction and oxidation of the catalyst. A reduced surface consists of mostly Cu-Zn active sites and an oxidized surface of Cu-O-Zn centers. They showed that after reduction the CO_2 hydrogenation activity is much higher than the CO hydrogenation. For an oxidized catalyst surface the CO hydrogenation is dominant. Kinetic isotope effects (KIE) and thermodynamic isotope effects (TIE) studies by Kunkes et al. [29] showed that CO is not formed by decomposition of methanol, but by the RWGS reaction. They also concluded that the formation of methanol and CO do not share a common intermediate. Thereby supporting the view that formate hydrogenation is the rate-determining-step (RDS) in methanol formation from CO_2 . The carboxyl decomposition or the CO_2 dissociation on the catalyst surface is proposed as the RDS for the RWGS reaction. The pathway from CO_2 to methanol is not through a consecutive RWGS and CO hydrogenation step [29]. Studies [30] using inelastic neutron scattering showed that under CO/H_2 conditions the surface contains methoxy and hydroxyl as stable surface intermediates, while under CO_2/H_2 conditions formate is also present.

Seidel et al. [20] and Park et al. [31] introduced kinetic models that

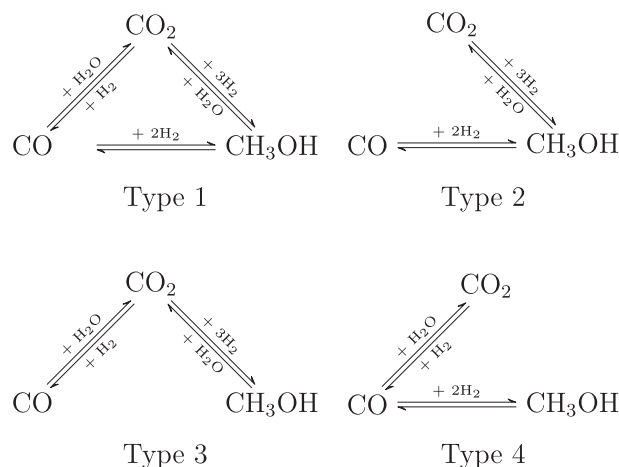


Fig. 1. Reaction network of methanol synthesis in four types of kinetic models. Type 1: all pathways can be taken [19,20,23]. Type 2: methanol is produced from both CO and CO_2 , while the RWGS reaction rate is not considered [21,24,25]. Type 3: methanol is only produced from CO_2 and the RWGS is considered for CO production [14–17]. Type 4: CO is considered as the main carbon source for methanol [13].

incorporate these different active centers for CO and CO₂, alongside a third center for H₂ adsorption. On top of this, the kinetic model of Seidel proposed a varying number of active centers (CO and CO₂) under changing gas phase compositions. They showed that the model has a good agreement with experimental data, although the temperature range of the experimental data does not include low temperatures (< 500 K), which is kinetically speaking most interesting.

1.2. Kinetic models

As Vanden Bussche and Froment [16] already pointed out before, a kinetic model for a methanol synthesis system that uses three rate equations (like Graaf et al. [19]) is predicting one surface concentration two times. This is not the case for the model by Seidel et al. [20], since they introduced the same surface species, but adsorbed on a different active surface center. The system can also be described by only two rate equations, since the third reaction is a sum of the other two. This is parameter wise more convenient, since less are needed. This reduces the identification problems with large amounts of fitting parameters as Seidel et al. pointed out. However, the model of Vanden Bussche and Froment [16] does not include the most recent developments and mechanistic insights from surface observations. Therefore a new kinetic model is here introduced, consistent with current insights from literature. With the focus on keeping the model as simple as possible, it was found to be possible to formulate the novel model in a form, related-but not identical to the original model of Vanden Bussche and Froment.

In this study, first the kinetic models of Graaf et al. [32] (Graaf), Vanden Bussche and Froment [16] (BF), Seidel et al. [20] (Seidel), Ma et al. [25] (Ma) and Villa et al. [13] (Villa) are refitted using a dataset of 234 experimental data points. In this way these models are compared in a fair manner on the same data set. The model proposed in this paper is also fitted and included in the comparison. Graaf, BF, Ma and Villa each have different underlying assumptions on the rate determining step (RDS) and active sites involved, while Seidel is the most recent model which includes current known physical effects. A screening is done with the proposed model to find the best matching RDS for this model. The experimental data set consists of 140 experiments by Seidel carried out in a backmixed (CSTR-type) contactor and 94 experiments (new data of this work) using a plug flow type (PFR) set-up. The total set covers the range of conditions of 453 to 573 K, 20 to 70 bar and GHSV of 2000 to 10,000, as shown in Fig. 2. The regression is done by global optimization using Matlab. The results are tested and validated using statistical methods. The goal is to present the most suitable and simple steady-state kinetic model for methanol synthesis over an industrial Cu/ZnO/Al₂O₃ catalyst.

2. Theory

In this section all kinetic models are presented for which the parameters are refitted. In every model the partial pressures are replaced by fugacities, afterwards the necessity for using fugacities is checked. The fugacities are calculated using the modified SRK equation of state, as presented by Van Bennekom et al. [33]. The reassessed relationships from Graaf and Winkelman [32] are used for calculating the equilibrium constants.

2.1. Graaf et al.

Graaf et al. [19] set up a kinetic model that includes three rate equations, one for CO hydrogenation (Eq. (4)), one for CO₂ hydrogenation (Eq. (5)) and the RWGS reaction (Eq. (6)). The model of Graaf uses two adsorption sites, which is reflected in Eq. (7) and (8). There is one adsorption site for CO and CO₂, and another site for H₂ and H₂O.

$$r_{CO} = k_{CO} K_{CO} \left(f_{CO} f_{H_2}^{\frac{3}{2}} - \frac{1}{K_{P_{CO}}(T)} \frac{f_{CH_3OH}}{f_{H_2}^{\frac{1}{2}}} \right) \Theta_{G_A} \Theta_{G_B} \quad (4)$$

$$r_{CO_2} = k_{CO_2} K_{CO_2} \left(f_{CO_2} f_{H_2}^{\frac{3}{2}} - \frac{1}{K_{P_{CO_2}}(T)} \frac{f_{CH_3OH} f_{H_2O}}{f_{H_2}^{\frac{3}{2}}} \right) \Theta_{G_A} \Theta_{G_B} \quad (5)$$

$$r_{RWGS} = k_{RWGS} K_{CO_2} \left(f_{CO_2} f_{H_2} - \frac{1}{K_{P_{RWGS}}(T)} f_{H_2O} f_{CO} \right) \Theta_{G_A} \Theta_{G_B} \quad (6)$$

$$\Theta_{G_A} = (1 + K_{CO} f_{CO} + K_{CO_2} f_{CO_2})^{-1} \quad (7)$$

$$\Theta_{G_B} = \left(f_{H_2}^{\frac{1}{2}} + \frac{K_{H_2O}}{K_{H_2}^{\frac{1}{2}}} f_{H_2O} \right)^{-1} \quad (8)$$

r_j is in mol/kg_{cat}s, the $K_{P_j}(T)$ parameters are the equilibrium constants as defined by Graaf and Winkelman [32]. The explanation of all (other) parameters can be found in the Nomenclature and all the original parameter values are in the Supporting information. The equations have been slightly adjusted to provide a uniform and comparable set of mathematic kinetic equations.

2.2. Vanden Bussche and Froment

Vanden Bussche and Froment [16] formulated a physically different kinetic model, assuming that there is only one active surface adsorption site for CO₂ hydrogenation and heterolytic decomposition of H₂. Next to this, they do not incorporate the direct CO hydrogenation reaction to

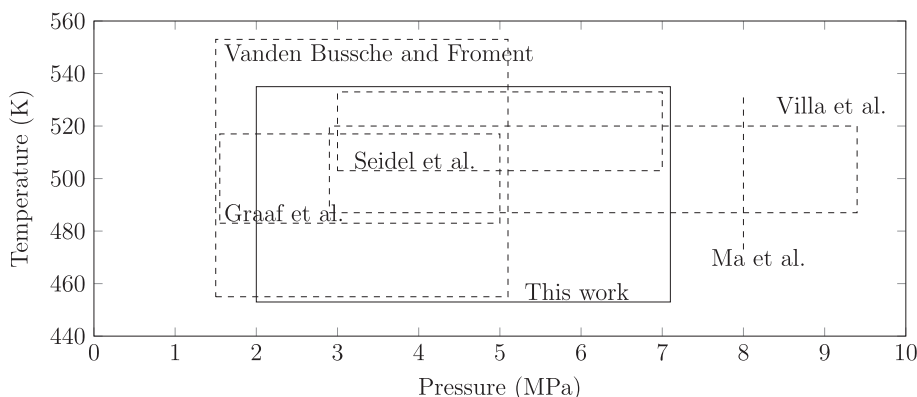


Fig. 2. Overview of the experimental temperature and pressure ranges used for fitting the kinetic models of Graaf et al. [19], Vanden Bussche and Froment [16], Ma et al. [25], Seidel et al. [20] and Villa et al. [13].

methanol. Their kinetic rate equations are given in Eqs. (9)–(11).

$$r_{CO_2} = k_{CO_2} f_{CO_2} f_{H_2} \left(1 - \frac{1}{K_{P_{CO_2}}(T)} \frac{f_{H_2O} f_{CH_3OH}}{f_{H_2}^3 f_{CO_2}} \right) \Theta_{BF}^3 \quad (9)$$

$$r_{RWGS} = k_{RWGS} f_{CO_2} \left(1 - \frac{1}{K_{P_{RWGS}}(T)} \frac{f_{H_2O} f_{CO}}{f_{CO_2} f_{H_2}} \right) \Theta_{BF} \quad (10)$$

$$\Theta_{BF} = \left(1 + \frac{K_{H_2O}}{K_8 K_9 K_{H_2}} \frac{f_{H_2O}}{f_{H_2}} + K_{H_2} f_{H_2}^{\frac{1}{2}} + K_{H_2O} f_{H_2O} \right)^{-1} \quad (11)$$

2.3. Seidel et al.

The kinetic model of Seidel et al. [20] takes three different active centers into account, denoted as follows:

1. \odot for oxidized surface centers, assumed as active center for CO-hydrogenation,
2. $*$ for reduced surface centers, assumed as active center for CO₂-hydrogenation,
3. \otimes as active surface centers for heterolytic decomposition of hydrogen.

These active surface centers are the basis for an elementary kinetic model. The authors describe two Langmuir-Hinshelwood models, a detailed one and a simplified one. They noted that with the detailed model the amount of fitting parameters is too high, so each individual parameter cannot be easily identified. Therefore, they introduced a simplified kinetic model. In this work only the simplified model is used, as it was shown by Seidel et al. that the simplified model fits their data equally well.

The rate equations of the simplified model are given in Eqs. (12)–(14).

$$r_{CO} = (1 - \phi) k_{CO} f_{CO} f_{H_2}^2 \left(1 - \frac{1}{K_{P_{CO}}(T)} \frac{f_{CH_3OH}}{f_{CO} f_{H_2}^2} \right) \Theta^{\odot} \Theta^{\otimes^4} \quad (12)$$

$$r_{CO_2} = \phi^2 k_{CO_2} f_{CO_2} f_{H_2}^2 \left(1 - \frac{1}{K_{P_{CO_2}}(T)} \frac{f_{CH_3OH} f_{H_2O}}{f_{CO_2} f_{H_2}^3} \right) \Theta^{*2} \Theta^{\otimes^4} \quad (13)$$

$$r_{RWGS} = \frac{\phi}{1 - \phi} k_{RWGS} f_{CO_2} \left(1 - \frac{1}{K_{P_{RWGS}}(T)} \frac{f_{CO} f_{H_2O}}{f_{CO_2} f_{H_2}} \right) \Theta^* \Theta^{\odot} \quad (14)$$

The surface coverages are given in Eqs. (15)–(17).

$$\Theta^{\odot} = (1 + K_{CO} f_{CO})^{-1} \quad (15)$$

$$\Theta^* = \left(1 + \frac{K_{H_2O} K_O}{K_{H_2}} \frac{f_{H_2O}}{f_{H_2}} + K_{CO_2} f_{CO_2} + K_{H_2O} f_{H_2O} \right)^{-1} \quad (16)$$

$$\Theta^{\otimes} = (1 + \sqrt{K_{H_2}} \sqrt{f_{H_2}})^{-1} \quad (17)$$

The ϕ constants (Eqs. (12) to (14)) do not match with the original paper [20], but have been corrected, according to correspondence with the author to be able to reproduce the results in the original paper.

The kinetic rate constants are calculated according to the reformulated Arrhenius-equation (Eq. (18)) [34].

$$k_j = \exp \left(A_j - B_j \left(\frac{T_{ref}}{T} - 1 \right) \right) \quad (18)$$

with $T_{ref} = 523.15$ K.

To describe the amount of relative surface centers the parameter ϕ_w is introduced. ϕ_w stands for the total amount of reduced centers and $1 - \phi_w$ is the total amount of oxidized centers. Seidel et al. used the

relation of Ovesen et al. [35] to calculate ϕ_w (Eqs. (19) and (20)).

$$\phi_w = \frac{1}{2} \left(1 - \frac{\gamma^*}{\gamma_0} \right) \quad (19)$$

with

$$\frac{\gamma^*}{\gamma_0} = \frac{1 - \sqrt{K_1 K_2 \frac{f_{H_2} f_{CO}}{f_{H_2O} f_{CO_2}}}}{1 + \sqrt{K_1 K_2 \frac{f_{H_2} f_{CO}}{f_{H_2O} f_{CO_2}}}} \quad (20)$$

The $\frac{\gamma^*}{\gamma_0}$ ratio is the relative surface contact free energy of Cu and Zn. This relation can be calculated from the surface geometries according to the Wulff construction framework. In the Seidel et al. kinetic model the K_1 and K_2 from Eq. (20) are calculated with Eqs. (21) and (22).

$$K_1 = \exp \left(\frac{-\Delta G_1}{RT} \right) \quad (21)$$

$$K_2 = \exp \left(\frac{-\Delta G_2}{RT} \right) \quad (22)$$

In Eq. (20) K_1 and K_2 are multiplied. In other words K_1 and K_2 are strongly correlated and K_3 can be defined as in Eq. (23).

$$K_3 = K_1 K_2 = \exp \left(\frac{-\Delta G_1 - \Delta G_2}{RT} \right) = \exp \left(\frac{\Delta G_3}{RT} \right) \quad (23)$$

From Eqs. (19), (20) and (23) ϕ_w is calculated. The ΔG_3 is fitted alongside the other parameters, since the concentrations of H₂ and H₂O are difficult to measure accurately. Only the steady-state model from Seidel et al. is considered. A maximum coverage of 90% reduced centers is assumed, as in the original work. Mathematically this is displayed in Eq. (24).

$$\phi = \phi_w - 0.1 \quad (24)$$

2.4. Ma et al.

The kinetic model of Ma et al. [25] includes two reaction rate terms, one for CO hydrogenation (25) and one for CO₂ hydrogenation (26). From Eq. (27) it can be derived that a single active site is assumed and that the overall reaction is taken as the rate determining step.

$$r_{CO} = k_{CO} f_{CO} f_{H_2}^2 \left(1 - \frac{1}{K_{P_{CO}}(T)} \frac{f_{CH_3OH}}{f_{CO} f_{H_2}^2} \right) \Theta_M^3 \quad (25)$$

$$r_{CO_2} = k_{CO_2} f_{CO_2} f_{H_2}^3 \left(1 - \frac{1}{K_{P_{CO_2}}(T)} \frac{f_{CH_3OH} f_{H_2O}}{f_{CO_2} f_{H_2}^3} \right) \Theta_M^4 \quad (26)$$

$$\Theta_M = (1 + K_{CO} f_{CO} + K_{CO_2} f_{CO_2} + K_{H_2} f_{H_2})^{-1} \quad (27)$$

2.5. Villa et al.

The kinetic model of Villa et al. [13,36] is composed of a model that includes two reaction rate terms, one for CO hydrogenation (28) and one for the RWGS (29). The adsorption term for methanol is neglected in Eq. (30), since after parameter estimation Villa et al. concluded that this had no influence.

$$r_{CO} = k_{CO} K_{CO} K_{H_2}^2 f_{CO} f_{H_2}^2 \left(1 - \frac{1}{K_{P_{CO}}(T)} \frac{f_{CH_3OH}}{f_{CO} f_{H_2}^2} \right) \Theta_V^3 \quad (28)$$

$$r_{RWGS} = k_{CO_2} K_{CO_2} K_{H_2} f_{CO_2} f_{H_2} \left(1 - \frac{1}{K_{P_{RWGS}}(T)} \frac{f_{CO} f_{H_2O}}{f_{CO_2} f_{H_2}} \right) \Theta_V^2 \quad (29)$$

$$\Theta_V = (1 + K_{CO} f_{CO} + K_{CO_2} f_{CO_2} + K_{H_2} f_{H_2})^{-1} \quad (30)$$

2.6. Proposed model

The proposed model is a Langmuir-Hinshelwood type model. The basis of the new model is the model of Vanden Bussche and Froment [16]. But instead of having one active site, three active surface centers (denoted as in the model of Seidel *, \odot and \otimes) are introduced [20]. Next to the three active centers the reactions can also be described by just two active centers, one for hydrogen and one for all other species. Both are tested in the screening, which is explained in the later Section 2.7. The mechanism for the RWGS is either the dissociation of CO_2 on the catalyst surface or the decomposition of adsorbed COOH [29]. Both are also evaluated in the screening. The corresponding elementary reaction steps are given in Table 1 for the methanol formation and Table 2 for the CO formation. The elementary reaction steps are adapted from Vanden Bussche and Froment with updates from recent literature. For instance, Grabow and Mavrikakis [37] pointed out that the CO_3^{**} intermediate does not play a role. Also the hydrogenation of formate leads to HCOOH , although mathematically this cannot be distinguished, so it is out of the scope of this article to postulate completely correct forms of intermediates. The full derivation of the model is given in the Supporting information. Aiming to arrive at a set of model parameters which are statistically meaningful, an effort is made to reduce the number of parameters as much as possible. This resulted in two models: a first model with 10 parameters, which is mechanistically in line with all observations mentioned in literature (physically correct) and a second with only 6 parameters that includes simplifying assumptions on the physical behavior. Both are shown here and in the results (Section 5).

2.6.1. Model derivation

The kinetic rate equation is based on the elementary pathways as shown in Table 1. The formate hydrogenation (reaction 3) is taken as the RDS for example, since it is often mentioned to be the RDS [29]. In this example derivation the CO_2 dissociation (reaction 12 in Table 2) is taken as the RDS for the RWGS reaction. The derived equations are shown in Eq. (31) and (32) for the 10-parameter model. The full derivation is given in the Supporting information.

$$r_{\text{CO}_2} = k_{\text{CO}_2} K_{\text{H}_2} f_{\text{CO}_2} f_{\text{H}_2} \left(1 - \frac{1}{K_{\text{P}_{\text{CO}_2}}(T)} \frac{f_{\text{CH}_3\text{OH}} f_{\text{H}_2\text{O}}}{f_{\text{H}_2}^3 f_{\text{CO}_2}} \right) \Theta^* \Theta^\otimes \quad (31)$$

where $k_{\text{CO}_2} = k_3^+ c_{*,t}^2 c_{\otimes,t} K_2$.

$$r_{\text{RWGS}} = k_{\text{RWGS}} f_{\text{CO}_2} \left(1 - \frac{1}{K_{\text{P}_{\text{RWGS}}}(T)} \frac{f_{\text{CO}} f_{\text{H}_2\text{O}}}{f_{\text{CO}_2} f_{\text{H}_2}} \right) \Theta^* \Theta^\odot \quad (32)$$

where $k_{\text{RWGS}} = k_{12}^+ c_{*,t} c_{\odot,t} K_{11}$.

According to catalyst surface measurements, hydroxyl, methoxy and formate groups are most abundant on the surface [30]. Therefore, all other surface species are neglected and a balance is set-up, as shown in Eq. (33).

$$c_{*,t} = c_* + c_{\text{OH}*} + c_{\text{H}_3\text{CO}*} + c_{\text{HCO}_2**} \quad (33)$$

Methoxy is assumed to adsorb on the reduced active centers, because it was pointed out by Kandemir et al. that it seems that the formate and methoxy species compete for the same sites [30]. The concentration of formate species (c_{HCO_2**}) is omitted, based on statistical significance criteria, see Supporting information. When the balance of Eq. (33) is solved the fraction of free reduced active sites can be found (Eq. (34)). The same balance is made and solved for oxidized active centers (Eq. (36)) and the hydrogen centers (Eq. (35)).

$$\Theta^* = \left(1 + \frac{f_{\text{H}_2\text{O}} K_{\text{H}_2\text{O}}}{\sqrt{f_{\text{H}_2}} K_{\text{H}_2} K_9} + \frac{f_{\text{CH}_3\text{OH}} K_{\text{CH}_3\text{OH}}}{\sqrt{f_{\text{H}_2}} K_{\text{H}_2}} \right)^{-1} \quad (34)$$

$$\Theta^\otimes = (1 + \sqrt{f_{\text{H}_2}} K_{\text{H}_2})^{-1} \quad (35)$$

$$\Theta^\odot = 1 \quad (36)$$

Since there were no observed surface species associated with the oxidized active center, Θ^\odot becomes one. The above model contains 10 parameters. $K_{\text{H}_2\text{O}}/K_9$ and $K_{\text{CH}_3\text{OH}}$ are both adsorption isotherms as defined in Eq. (45).

The number of parameters is further reduced by the assumption that the hydrogen active sites are always occupied [19]. This assumption holds in any reactor where hydrogen is abundant on a molar basis. With the assumption that adsorption isotherms are linearly dependent on each other (Eqs. (37) and (38)), the need for fitting separate Arrhenius equations is eliminated and only the 'ratios' ($k_{\text{H}_2\text{O}/9}$; k_{H_2} : ($k_{\text{MeOH}} = 1$)) of surface coverage are left over. The hydrogen and methanol adsorption isotherms are now lumped under the k_{CO_2} and k_{RWGS} . Or in other words, the proposed kinetic model is reduced to only two temperature dependencies, one for each reaction rate. This means that the overall observed rate at a specific temperature is the sum of the temperature dependence of the adsorption isotherms and the reaction rate itself. This matches with experimental observations, since at a single temperature only the reaction rates are measured. The $k_{\text{H}_2\text{O}/9}$ and k_{H_2} are the regressed constants that can be used to get an estimate of the respective adsorption isotherms via Eqs. (37) and (38), if the (temperature dependent) adsorption isotherm of methanol is known. Because of these parameter reductions the unit of Θ^* changed from a fraction to bar^{-1} . Therefore, Θ^* is introduced which can be interpreted as the fugacity dependent free surface coverage.

$$k_{\text{H}_2\text{O}/9} = \frac{K_{\text{H}_2\text{O}}}{K_9 K_{\text{CH}_3\text{OH}}} \quad (37)$$

$$k_{\text{H}_2} = \frac{\sqrt{K_{\text{H}_2}}}{K_{\text{CH}_3\text{OH}}} \quad (38)$$

Therefore, a model with a reduced number of parameters, consisting of the kinetic rate Eqs. (39)–(41), having only 6 fitting parameters is here proposed.

$$r_{\text{CO}_2} = k_{\text{CO}_2} f_{\text{CO}_2} f_{\text{H}_2}^{\frac{3}{2}} \left(1 - \frac{1}{K_{\text{P}_{\text{CO}_2}}(T)} \frac{f_{\text{CH}_3\text{OH}} f_{\text{H}_2\text{O}}}{f_{\text{H}_2}^3 f_{\text{CO}_2}} \right) \Theta^{*2} \quad (39)$$

where k_{CO_2} is a lumped fitting parameter representing $k_3^+ c_{*,t}^2 c_{\otimes,t} K_{\text{H}_2}^{\frac{3}{2}} K_2 K_{\text{CH}_3\text{OH}}^{-2}$.

$$r_{\text{RWGS}} = k_{\text{RWGS}} f_{\text{CO}_2} f_{\text{H}_2}^{\frac{1}{2}} \left(1 - \frac{1}{K_{\text{P}_{\text{RWGS}}}(T)} \frac{f_{\text{CO}} f_{\text{H}_2\text{O}}}{f_{\text{CO}_2} f_{\text{H}_2}} \right) \Theta^* \quad (40)$$

where $k_{\text{RWGS}} = k_{12}^+ c_{*,t} c_{\odot,t} K_{11} K_{\text{H}_2}^{\frac{1}{2}} K_{\text{CH}_3\text{OH}}^{-1}$ and with:

Table 1

Simplified elementary reaction steps for the proposed kinetic model for methanol formation [16,37]. Three active sites are considered. The actual form and positions of an intermediate on the surface is neglected, because it has no influence on the equations.

Reaction	Elementary reaction step	Equilibrium constant
<i>CO₂ hydrogenation</i>		
1	$\text{H}_2(\text{g}) + 2 \otimes \rightleftharpoons 2\text{H}\otimes$	K_{H_2}
2	$\text{CO}_2(\text{g}) + 2 * + \text{H}\otimes \rightleftharpoons \text{HCO}_2 **$	K_2
3	$\text{HCO}_2 ** + \text{H}\otimes \rightleftharpoons \text{HCOOH} ** + \otimes$	K_3
4	$\text{HCOOH} ** \rightleftharpoons \text{HCO} * + \text{OH} *$	K_4
5	$\text{HCO} * + \text{H}\otimes \rightleftharpoons \text{H}_2\text{CO} * + \otimes$	K_5
6	$\text{H}_2\text{CO} * + \text{H}\otimes \rightleftharpoons \text{H}_3\text{CO} * + \otimes$	K_6
7	$\text{H}_3\text{CO} * + \text{H}\otimes \rightleftharpoons \text{CH}_3\text{OH}(\text{g}) + * + \otimes$	K_7
<i>Water formation</i>		
8	$\text{O} * + \text{H}\otimes \rightleftharpoons \text{OH} * + \otimes$	K_8
9	$\text{OH} * + \text{H}\otimes \rightleftharpoons \text{H}_2\text{O} * + \otimes$	K_9
10	$\text{H}_2\text{O} * \rightleftharpoons \text{H}_2\text{O}(\text{g}) + *$	K_{10}

Table 2

Elementary reaction steps for the proposed kinetic model for CO formation. Three active sites are considered.

Reaction	Elementary reaction step	Equilibrium constant
<i>RWGS reaction – CO₂ dissociation</i>		
11	$\text{CO}_2(\text{g}) + * \rightleftharpoons \text{CO}_2^*$	K_{11}
12	$\text{CO}_2^* + \odot \rightleftharpoons \text{CO} \odot + \text{O}^*$	K_{12}
13	$\text{CO} \odot \rightleftharpoons \text{CO}(\text{g}) + \odot$	K_{13}
<i>RWGS reaction – COOH decomposition</i>		
14	$\text{CO}_2^* + \text{H} \otimes \rightleftharpoons \text{COOH}^* + \otimes$	K_{14}
15	$\text{COOH}^* + \odot \rightleftharpoons \text{CO} \odot + \text{OH}^*$	K_{15}
<i>RWGS reaction – * and \odot similar sites</i>		
16	$\text{CO}_2^* + * \rightleftharpoons \text{CO}^* + \text{O}^*$	K_{16}
17	$\text{CO}^* \rightleftharpoons \text{CO}(\text{g}) + *$	K_{17}
18	$\text{COOH}^* + * \rightleftharpoons \text{CO}^* + \text{OH}^*$	K_{18}

$$\theta^* = \left(f_{\text{H}_2}^{\frac{1}{2}} k_{\text{H}_2} + f_{\text{H}_2\text{O}} k_{\text{H}_2\text{O}/9} + f_{\text{CH}_3\text{OH}} \right)^{-1} \quad (41)$$

In Eqs. (39) and (40) f_i is in bar and r_i is in mol/kg_{cat}s. k_{CO_2} and k_{RWGS} are both described using the Arrhenius equation (Eq. (46)). k_{H_2} and $k_{\text{H}_2\text{O}/9}$ are constants. In the results sections the two models are distinguished by the number of parameters ($N_p = 6$ or 10). The powers of the hydrogen partial pressures and the fraction of free sites in Eqs.

(39) and (40) can still change based on which RDS is found as the most optimal.

2.7. Rate determining step

Next to the underlying mechanisms, as explained in Section 1.1, each model also has its own assumption about the number of kinetic sites and rate determining steps. An overview of all pathways is given in Fig. 3. The elementary pathways for the models of Ma et al. and Villa et al. are not given in the original work. From their model equations it can be seen that the kinetic models are formulated from the overall reaction and not based on intermediate reactions on the surface. Opposed to taking the commonly known RDS for methanol synthesis [19,38], in this work a screening effort is made. The RDS for the proposed 6-parameter model is screened by regression of all possible steps (Table 1 and 2) as the rate determining one. All of the mathematical equations are given in Table 3. They result in a total combination of 30 unique models. The RDS found in evaluating the options for the 6-parameter model is also used for the 10-parameter model.

3. Experiments

The experimental data of this work is divided in two groups. Experiments were carried out at both the University of Twente (The Netherlands) and at the Kemijski inštitut (Slovenia).

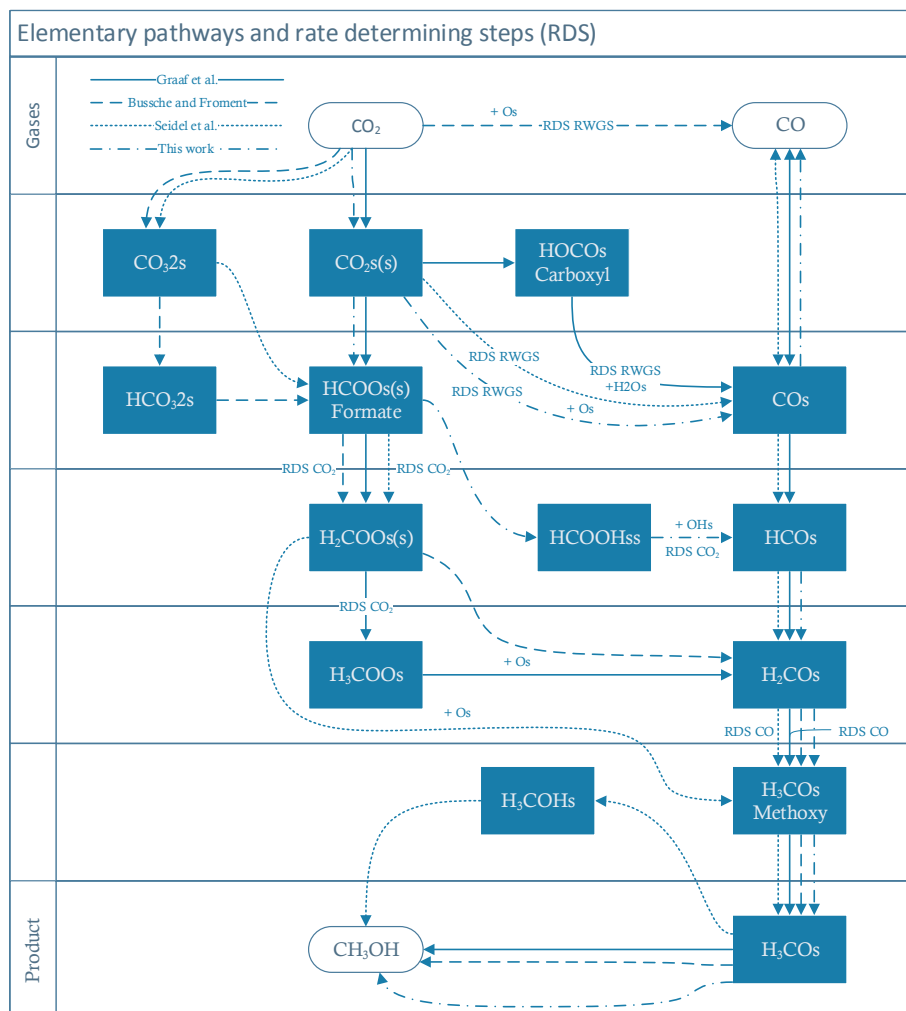


Fig. 3. Elementary pathways and rate determining steps of the kinetic models from Graaf et al. [19], Vanden Bussche and Froment [16], Seidel et al. [20] and this work. The RDS shown for this work comes from the result Section 5.1.

Table 3

Evaluation scheme for the screening of the rate determining step using the six parameter model. Reactions are defined in Tables 1 and 2.

Reaction	Rate determining step
	<i>CO₂ hydrogenation</i>
2	$r_{CO_2} = k_{CO_2} f_{CO_2} f_{H_2} \left(1 - \frac{1}{K_{PCO_2}(T)} \frac{f_{CH_3OH} f_{H_2O}}{f_{H_2}^3 f_{CO_2}} \right) \theta^2$
3	$r_{CO_2} = k_{CO_2} f_{CO_2} f_{H_2}^{\frac{3}{2}} \left(1 - \frac{1}{K_{PCO_2}(T)} \frac{f_{CH_3OH} f_{H_2O}}{f_{H_2}^3 f_{CO_2}} \right) \theta^2$
4	$r_{CO_2} = k_{CO_2} f_{CO_2} f_{H_2}^2 \left(1 - \frac{1}{K_{PCO_2}(T)} \frac{f_{CH_3OH} f_{H_2O}}{f_{H_2}^3 f_{CO_2}} \right) \theta^2$
5	$r_{CO_2} = k_{CO_2} f_{CO_2} f_{H_2}^{\frac{3}{2}} \left(1 - \frac{1}{K_{PCO_2}(T)} \frac{f_{CH_3OH} f_{H_2O}}{f_{H_2}^3 f_{CO_2}} \right) \theta^*$
6	$r_{CO_2} = k_{CO_2} f_{CO_2} f_{H_2}^2 \left(1 - \frac{1}{K_{PCO_2}(T)} \frac{f_{CH_3OH} f_{H_2O}}{f_{H_2}^3 f_{CO_2}} \right) \theta^*$
7	$r_{CO_2} = k_{CO_2} f_{CO_2} f_{H_2}^{\frac{5}{2}} \left(1 - \frac{1}{K_{PCO_2}(T)} \frac{f_{CH_3OH} f_{H_2O}}{f_{H_2}^3 f_{CO_2}} \right) \theta^*$
	<i>RWGS reaction – CO₂ dissociation</i>
11	$r_{RWGS} = k_{RWGS} f_{CO_2} f_{H_2}^{\frac{1}{2}} \left(1 - \frac{1}{K_{PRWGS}(T)} \frac{f_{CO} f_{H_2O}}{f_{CO_2} f_{H_2}} \right) \theta^*$
12	Equal to reaction 11
13	$r_{RWGS} = k_{RWGS} f_{CO_2} \left(1 - \frac{1}{K_{PRWGS}(T)} \frac{f_{CO} f_{H_2O}}{f_{CO_2} f_{H_2}} \right)$
	<i>RWGS reaction – COOH decomposition</i>
14	Equal to reaction 11
15	$r_{RWGS} = k_{RWGS} f_{CO_2} f_{H_2} \left(1 - \frac{1}{K_{PRWGS}(T)} \frac{f_{CO} f_{H_2O}}{f_{CO_2} f_{H_2}} \right) \theta^*$
	<i>RWGS reaction – * and ⊙ similar sites</i>
16	$r_{RWGS} = k_{RWGS} f_{CO_2} f_{H_2} \left(1 - \frac{1}{K_{PRWGS}(T)} \frac{f_{CO} f_{H_2O}}{f_{CO_2} f_{H_2}} \right) \theta^2$
17	Equal to reaction 11
18	$r_{RWGS} = k_{RWGS} f_{CO_2} f_{H_2}^{\frac{3}{2}} \left(1 - \frac{1}{K_{PRWGS}(T)} \frac{f_{CO} f_{H_2O}}{f_{CO_2} f_{H_2}} \right) \theta^2$

3.1. Experiments at Kemijski inštitut

The first and largest group is data produced, using the facilities of the National Institute of Chemistry of Slovenia, Kemijski inštitut. The set-up consists of four parallel isothermal fixed beds. More details can be found in several papers [39,40]. Experiments performed range from 483 K to 533 K, 20 and 50 bara and 2000 to 10,000 GHSV. Dimensions for this reactor are $6.35 \cdot 10^{-3}$ m in diameter and $3.16 \cdot 10^{-2}$ m in length. The amount of catalyst (Johnson Matthey, CP-488) varies per reactor per experimental point and can be found in the Supporting information.

3.2. Experiments at the University of Twente

The second group of experiments are performed at the University of Twente, using the fixed bed setup shown in Fig. 4. Premixed gas (MG) is supplied from a gas bottle and preheated before it enters the isothermal catalyst bed. Product vapors are condensed and collected in a small reservoir (E-6, Fig. 4), while non-condensable gases leave the system by the gas flow meter (GM-1, Fig. 4). The flow-sheet is discussed in more detail below.

The top section of the flow scheme includes the feed gas preparation. The flow of each individual gas feed is regulated by a mass flow controller (MFC-1 to MFC-5) (Brooks Instruments, 5850TR). All gas feeds mix in a central tube located in the pre-heater block (E-1) controlled by an Eurotherm 2132 PID controller. A pressure sensor (PI-1) (GE Oil & Gas, Unik PTX-7517-3257) measures the inlet pressure.

The Cu/ZnO/Al₂O₃ methanol catalyst (Johnson Matthey, CP-488) is

crushed and loaded into a 0.67 m long quartz tube (E-4) with $3 \cdot 10^{-3}$ m internal diameter. The insert in Fig. 4 shows the layout of the quartz tube and the positioning of the thermocouples. The catalyst bed is 0.28 m long and contains 1.54 g of catalyst. Two centimeters of quartz wool keeps the catalyst in position and ensures equal gas distribution. The quartz tube is placed in a metal tube (Inconel 600) (E-3). The metal tube is enclosed by two heaters in an isolation shell [E-2].

Vapor products are condensed in the shell and tube condenser (E-5) with water as coolant. Liquid products are collected in a small reservoir (E-6) and can be removed from the setup by opening V-13. The temperature (TI-3) and pressure (PI-2) after the reactor are monitored. A back pressure controller (BPC) regulates the pressure in the reactor. Pressure sensor PI-3 and PI-4 indicate the pressure directly after the BPC and before the gas meter, respectively. Needle valve V-15 is adjusted so a pressure around 0.3 barg is created to transport the product gases to the GC (E-7). When no gas samples are taken the product gases leave the setup by the gas meter (GM) (Ritter, TG0.5-1.4571-PVC). Temperature sensor TI-4 is used to correct the gas flow for temperature. Gas composition was determined using gas chromatography (Varian 450-RGA). The GC is equipped with three channels. Channel 1 analyses hydrogen using TCD detection on a Haysep Q column (Agilent CP1305) and a Molsieve 5A column (Agilent CP1306) using N₂ as carrier gas. Channel 2 detects permanent gases using TCD detection on a Haysep Q column (Varian CP1308), Haysep N column (Varian CP1307) and a Molsieve 13X column (Varian CP1309) using helium as carrier gas. Channel 3 detects hydrocarbons using FID detection using a CP-Sil 5CB column (Varian CP1310) and a Select Al₂O₃/MAPD column (Varian CP7433) using helium as carrier gas. The reactor is directly connected to the GC and the tubing between the GC and setup are flushed using N₂ between gas samples.

The liquid product was analyzed in a HPLC (Agilent Technologies 1200 Series) using RID detection and GROM Resin H + IEX column equipped with a pre-column. The injected volume was 10 μL, the temperature 65°C and the mobile phase 5 mM H₂SO₄ at 0.6 mL min⁻¹. Calibration curves were obtained by injecting mixtures of known composition (Sigma Aldrich HPLC grade Methanol and milliQ ultrapure water) in the range of interest.

3.3. Experimental method

First the cooling water is switched on and the mix gas MFC is set to the targeted gas flow. The system is pressurized using the feed gas, after which it will flush the system. Heaters are switched on and the system is stabilized for at least 30 min after reaching the set point conditions. At the start of the experiment liquid is drained from the collection vessel. At the end of an experiment the weight of the total collected liquid is measured on an analytical balance (Mettler AE 160). The conversion of CO₂ is determined by the gas composition and the total outlet gas flow. Selectivity is determined by the gas composition of CO assuming methanol and CO being the only products. Experiments are performed between 451 K and 523 K, 20 to 50 bara and at a constant flow of 3000 GHSV.

4. Parameter estimation

The reactor model (Eq. (42)) consists of an isothermal plug flow pseudo-homogeneous model [41]. The presence of external and internal mass transfer limitations are checked using respectively the Mears' and Weisz-Prater criterion [42,43]. The criteria were met for all experimental conditions applied. Heat effects are neglected, in view of the small diameter of the quartz tube. Axial, radial, intra- and gas-particle heat and mass transfer limitations were calculated for the set-up at the Kemijski inštitut and all criteria were met.

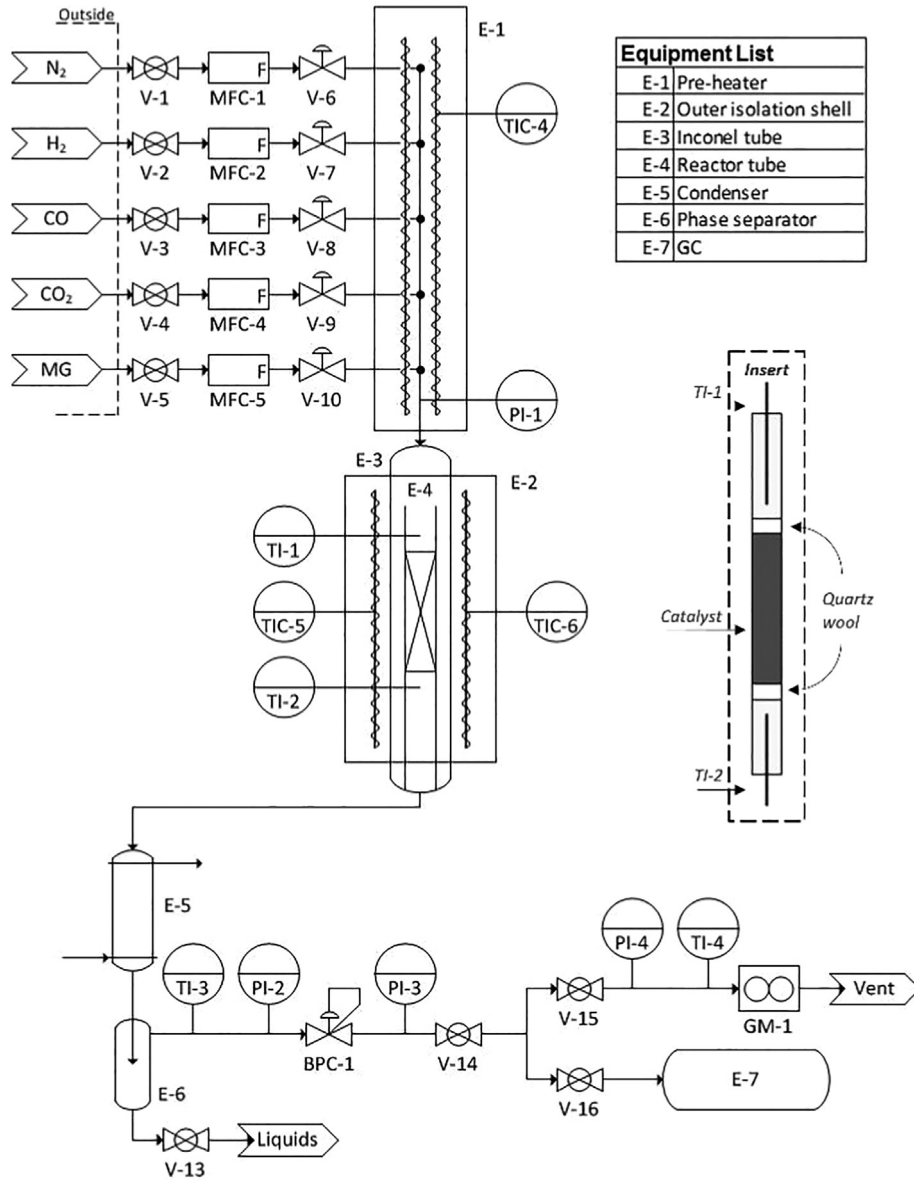


Fig. 4. Experimental setup for the kinetic experiments. The insert shows the positioning of the catalyst bed and thermocouples inside the reactor.

$$\frac{\phi_m}{A_r} \frac{dw_i}{dx} = M_{wi} \sum_{j=1}^3 \nu_{i,j} (1 - \epsilon_b) \rho_{cat} r_j \quad (42)$$

All of the parameters for the models of Graaf, BF, Seidel, Ma and Villa are refitted. The Arrhenius equations for adsorption constants are rewritten in its logarithmic form (Eq. (43)). The same is done for the kinetic rate constants (Eq. (44)) to improve numerical sensitivity. All constants are back calculated to the original Arrhenius form (Eqs. (45) and (46)).

$$\ln(K_i) = a_i - b_i T^{-1} \quad (43)$$

$$\ln(k_i) = a_i - b_i T^{-1} \quad (44)$$

$$K_i = A_i \exp\left(\frac{B_i}{RT}\right) = \exp\left(\frac{\Delta S_{ads}^\circ}{R}\right) \exp\left(\frac{-\Delta H_{ads}^\circ}{RT}\right) \quad (45)$$

$$k_i = A_i \exp\left(\frac{B_i}{RT}\right) = A \exp\left(\frac{-E_A}{RT}\right) \quad (46)$$

where $A_i = \exp(a_i)$ and $B_i = -b_i R$. The A_j and B_j coefficients of Seidel are regressed in the same way, but the original equation is used (Eq.

(18)). The constants A_i and B_i in Eq. (46) can be calculated back from Eq. (18) with $A_i = \exp(A_j + B_j)$ and $B_i = -B_j T_{ref} R$.

To arrive at physically meaningful values for the model parameters, the following checks and bounds are applied [16,19,44]:

- Rule 1: $k > 0$ and $K > 0$, imposed by logarithmic Arrhenius form
- Rule 2: $E_A > 0$ or $b_i > 0$, imposed by bounds
- Rule 3: $-\Delta H_{ads}^\circ > 0$ or $b_i < 0$, imposed by bounds
- Rule 4: $0 < -\Delta S_{ads}^\circ < S_{gas}^\circ$, checked afterwards

When the ingoing concentration of a component is zero, mathematically still a minimum (non-zero) value is required. Otherwise, the reaction rate constant is zero for models like BF, Seidel and the proposed model. A significant change in parameters is observed below 50 ppm, so 50 ppm is used as the inlet concentrations when the actual concentration is zero.

4.1. Regression method

The parameter estimation is done with the χ^2 (chi-Square)

regression method. The quantity of χ^2 is a sum of the residual squared errors summed over N measurements and normalized on the unit standard deviation, as shown in Eq. (47). The global minimum is found by using the Global Optimization Toolbox of MATLAB® 2017b. GlobalSearch is initiated with the fmincon solver and the Sequential Quadratic Programming (SQP) algorithm. The bounds are set as discussed in Section 4 to produce physically correct solutions.

$$\chi^2 = \sum_{j=1}^N \sum_{i=1}^{N_c} \left(\frac{w_i - \hat{w}_i}{\sigma_{w_i}} \right)^2_j \quad (47)$$

The weighing factor σ_{w_i} from Eq. (47) is based on the experimental error and is calculated for each experiment. It is composed of the standard deviation of the calibration curve of the GC plus the standard deviation of at least three GC measurements per experiment. The standard deviation of the measured flows and feed compositions are also taken into account. For the experiments of Seidel it is assumed that each component has a standard deviation of 0.002 in mole fraction. All values can be found in the Supporting information.

The mean squared error (MSE) is defined as in Eq. (48). It is shown for comparison between regression with and without errors.

$$MSE_k = \frac{1}{N} \frac{1}{N_c} \sum_{j=1}^N \sum_{i=1}^{N_c} (w_i - \hat{w}_i)^2_j \quad (48)$$

4.2. Cross-validation statistical method

To statistically determine a good fit with uncertainty boundaries, the 5-fold Cross-Validation (CV) method is used [45]. The method introduces a training set for model regression and a test set for validation. The total dataset as described in Section 3 is divided into five random folds (groups). Five unique training sets are created when one fold is taken out each time. The training set consisting of four folds is used for fitting the model. The test set consisting of one fold is used for validation.

There are two purposes of this method. The first is to determine how well each model predicts data points outside its trained dataset. Secondly, it tells how much the parameters deviate when fitted on a specific dataset, because five fits are obtained from essentially the same dataset, instead of the traditional single fit with 95% confidence bounds.

$$CV_{(5)} = \frac{1}{5} \sum_{k=1}^5 \chi_k^2 \quad (49)$$

The mean of the five test χ^2 's give an indication of the prediction outside the training set (Eq. (49)). The model with the lowest $CV_{(5)}$ is the best predictive model. From each model the χ^2 is calculated over the total dataset for each of the five fits and the lowest one (called χ_{best}^2) is presented as the best fit per model. This is done to present the absolute best model and to prevent averaging parameters which are correlated, such parameters will show a large standard deviation.

This method is used to get a clear image about the predictive capabilities ($CV_{(5)}$) and the ability to fit a known dataset (χ_{best}^2). A kinetic model should be good in predicting, rather than fitting a known dataset extremely well. In this light and as a final test for all models the experiments of Gaikwad et al. [46] are used to check for predictability completely outside the fitted region. Gaikwad et al. performed experiments at very high pressures and space velocities (up to 442 bar and 100,000 GHSV). Such experiments are not present in the current work.

The standard deviation of each model parameter is calculated as the standard deviation over the five fits. The average deviation of a model over five fits is captured in a single parameter as defined in Eq. (50).

$$\sigma_{p,avg} = \frac{1}{N_p} \sum_{i=1}^{N_p} \frac{\sigma_{p_i}}{|p_i|} \quad (50)$$

where p_i is the fitted parameter of the χ_{best}^2 fit. The higher $\sigma_{p,avg}$, the more on average the parameters are changing. Or in other words, when a completely new dataset is taken one can expect the same model to have a deviation of $\sigma_{p,avg}$ percent. This number should be low for a kinetic model, since in theory there is only one set of parameters.

$$K_{CC} = \frac{1}{N_p^2} \sum_{i=1}^{N_p} \sum_{j=1}^{N_p} |CC_{ij}| \quad (51)$$

A last statistical parameter introduced is the average correlation number of the cross-correlation matrix (CC). It is defined as in Eq. (51). The diagonals are set to zero instead of one. This results in a K_{CC} value between zero and one for any model with any amount of parameters, just like the cross-correlation values itself.

5. Results and discussion

The regression of all kinetic models on the 234 experiments was successful and the resulting regressed values of the parameters are presented for each model in the Supporting information. Next to the physical models presented here also a power law as described by Kobl et al. [47] was tested using the CV method, the results are given in the Supporting information. The outcome is that a power law cannot predict the full dataset. First the results of the screening of the rate determining steps (RDS) are discussed and subsequently the results of the full comparison of the kinetic models of Graaf, BF, Seidel, Ma, Villa, the 10-parameter model and the 6-parameter model both with the RDS as found in the screening.

5.1. RDS screening

The most interesting results of the screening are given in Table 4, the rest is given in the Supporting information. Many RDSs tested do not lead to good data fits. The best matching RDS is reaction 4, being the dissociation of OH from HCOOH, for the CO₂ hydrogenation. Reactions 11, 12, 14 or 17 are the best match for the RWGS reaction. Mathematically, no distinction can be made between the four RWGS reactions, but reaction 11, 14 and 17 are not commonly assumed as the RDS in literature. Whilst reaction 12 is proposed by others as RDS and this is further supported by kinetic isotope effect measurements [20,29]. The other RDS, the COOH decomposition, as suggested by Kunkes et al. [29], leads to a data fit that is statistically almost as good as the CO₂ dissociation RDS, but the regression is simply a bit lower.

Interestingly, the most commonly assumed RDS for CO₂ hydrogenation comes at a second place, right after the dissociation of OH from HCOOH. DFT calculations have shown more insight into the different pathways and also found opposing results. Zhao et al. [48]

Table 4

Top five screening results of the rate determining steps plus other important results, the rest is available in the Supporting information. The best match is the dissociation of the oxygen from formate, instead of the most commonly used formate hydrogenation as a RDS. The selected RDSs are highlighted in bold.

Reaction number		χ_{best}^2 ($\cdot 10^4$)	MSE_{best} ($\cdot 10^{-5}$)	$CV_{(5)}$ ($\cdot 10^4$)	MSE Gaikwad [46]
CO ₂ hydrogenation	RWGS				
Top 5					
4	11/12/14/17	1.80	1.81	1.92	1.7
4	15	1.83	1.64	2.45	1.7
7	18	1.86	1.76	7.76	1.7
3	11/12/14/17	1.88	1.82	1.95	2.4
3	15	2.04	1.74	0.89	2.5
3	18	2.17	1.68	1.11	2.7
3	16	2.32	1.66	4.42	2.3
4	16	2.81	1.82	52.71	2.2

pointed out that from their calculations it seems that the OH dissociation is even more difficult than the hydrogenation of formate. They, and others [49], also suggested that the formate pathway could be a dead end and that formate is just a spectator on the surface. It explains the possibility of having another RDS than the most obvious one based on experimental observations. But again, in these results statistically speaking the difference is still too small to distinguish either as the best.

The combination of formate hydrogenation (reaction 3) and COOH decomposition (reaction 15) is good in predicting within the own dataset. Unfortunately, it predicts the dataset of Gaikwad not as well. Therefore, simply the model with the lowest χ^2 is chosen (the top one in Table 4). This results in different equations, so the correct ones are (52), (40) and (41).

$$r_{\text{CO}_2} = k_{\text{CO}_2} f_{\text{CO}_2} f_{\text{H}_2}^2 \left(1 - \frac{1}{K_{\text{pCO}_2}(T)} \frac{f_{\text{CH}_3\text{OH}} f_{\text{H}_2\text{O}}}{f_{\text{H}_2}^3 f_{\text{CO}_2}} \right) \theta^{\#^2} \quad (52)$$

Another result from the screening is that three different active centers represent the dataset the best. When oxidized and reduced active centers are taken as one and the same (reactions 3 or 4 combined with 16 or 18) it seems that these do not represent the system as good as using different sites (reactions 3 or 4 combined with 11 or 15). The difference is the largest with 4 and 16 compared to 4 and 11. Also, the fact that the MSE can be lower for reaction 3 and 16 than the top fit shows the importance of the χ^2 to focus on the trend in the data and to prevent regression of experimental errors.

5.2. Model comparison

The statistics of the regression results are given in Table 5. The residual standard errors (RSE) is shown in the Supporting information. The original model of BF predicts the dataset better than the original Graaf model. This may be attributed to the fact that the model by Graaf was regressed on experiments with the older MK-101 catalyst and that catalysts over decades have improved in activity [50]. However, after regression of the model parameters, the Graaf model performs better. Seidel proved to be the best predictive model, since it has the lowest χ^2 and $CV_{(5)}$. BF and Graaf are good for fitting a known dataset, but not for predicting outside its training set, because the $CV_{(5)}$ values are higher. The reason could be that there is an incorrect physical assumption in the BF model and that there are too many parameters for the Graaf model so that it can provide a good fit, but not predict. The predictions by the models from Ma and Villa are significantly worse. From that it can be concluded that Type 2 and 4 models (see Fig. 1) do not represent the system well and can be disregarded. The models of Ma and Villa are not predicting nor fitting the experiments well. It can be concluded from this analysis that the RWGS reaction is too important in this system to neglect in the kinetic rate expression. Considering CO as the main source of methanol also cannot provide a universal model for both CO₂ and CO conversion to methanol.

It has to be checked whether the newly regressed parameters of the Seidel model do not give a worse prediction than the original prediction of their own dataset. To be able to do that a χ^2 value is calculated for only the data of Seidel et al. Then these values are compared for the original parameters and the regressed parameters. The original model has a $\chi_{\text{Seidel,orig}}^2$ of $4.8 \cdot 10^3$ versus the new regressed parameters with $\chi_{\text{Seidel}}^2 = 3.7 \cdot 10^3$. This means that the new parameters provide an even better prediction of their original dataset plus a significantly better prediction of the dataset from this work, as shown in Table 5. The biggest deviation from the original parameters are for the constants ΔG_3 , k_{CO_2} B and $K_{\text{H}_2\text{O}}$, which can be found in the Supporting information. The fact that they could predict their data with a completely different set of parameters indicates that a much larger and unique dataset is required to regress a 12 parameter model. By adding more data in this paper a step forward is made to their model.

Other than the Ma and Villa models, all other models predict the

complete dataset well. This is an interesting outcome, since Seidel assumed three different active sites, Graaf two sites and BF only one active site. This means that based on this dataset, no clear distinction can be made between these mechanics. BF cannot predict the experiments with a feed of pure CO as well as the other models. This indicates that at least two different active sites must be taken into account, since the other models can predict these compositions. At high pressure BF is also not able to predict correctly, this is shown in Fig. 6. BF predicts a constant response on the conversion of CO₂ for higher pressures. This is not to be expected, based on experimental findings and is also reflected in the high MSE of the experiments from Gaikwad et al. [46]. The differences between Graaf, Seidel and the novel 10-parameter model are small, meaning no distinction can be made on whether two or three different active sites are better representing the actual situation. However, one must also keep in mind that these models have a high amount of parameters and that the $\sigma_{p,\text{avg}}$ is high for Graaf and the 10-parameter model. The high $\sigma_{p,\text{avg}}$ means that each of the five fits gave a different set of parameters, which could individually fit the experiments in that dataset well. It might be that models with this many parameters are just good at fitting experimental data, without requiring the underlying model to be physically correct, because Graaf is fundamentally very different from Seidel and this work. The $\sigma_{p,\text{avg}}$ for Seidel is lower, which might be an indication that the model has better physical assumptions.

The covariance of the parameters from the 6-parameter model is shown in Table 6 in the form of the cross-correlation matrix. The pre-exponential factors are completely correlated to the activation energies. A high correlation between those is common in Arrhenius type equations. The rest of the parameters are not correlated, which is also reflected in the lowest K_{CC} value in Table 5. For comparison the cross-correlation matrix of the 10-parameter model is given in the Supporting information. But also the higher K_{CC} indicates more cross-correlation.

The low cross correlation and the low amount of parameters show that the major physical effects are included in the 6-parameter model. On top of that the $\sigma_{p,\text{avg}}$ is low, meaning that the model has a low variance and is not fitting the errors in the dataset. The bias of the model towards a certain behavior seems absent, as it also follows the expected trends just as well as the other models (Fig. 5 and 6). The conversion and selectivity in Fig. 5 and 6 are respectively defined as in Eqs. (53) and (54).

$$\zeta_{\text{CO}_2} = 1 - \frac{y_{\text{CO}_2,\text{out}}}{y_{\text{CO}_2,\text{in}}} \quad (53)$$

$$\sigma_{\text{MeOH}} = 1 - \frac{y_{\text{CO},\text{out}}}{y_{\text{CO}_2,\text{in}} - y_{\text{CO}_2,\text{out}}} \quad (54)$$

The low MSE for the data of Gaikwad et al. is proving that the model is a good predicting model, whereas larger parameter models like BF fail to predict outside their fitted domain. More experimental data is needed to fit for example hydrogen adsorption isotherms and be able to

Table 5

Comparison between the fitted kinetic models based on the $CV_{(5)}$ and the χ^2 . Also the model performance with original parameters (χ_{orig}^2) on this dataset is shown together with the number of parameters (N_p). All of the parameters of each model are refitted.

Type (Fig. 1)	Model	$CV_{(5)}$ ($\cdot 10^4$)	χ_{best}^2 ($\cdot 10^4$)	χ_{orig}^2 ($\cdot 10^4$)	$\sigma_{p,\text{avg}}$ (%)	N_p	K_{CC}	MSE Gaikwad [46]
1	Graaf	3.75	2.25	43.7	54	12	0.30	1.5
3	BF	4.07	3.20	18.7	62	9	0.31	14
1	Seidel	1.71	1.35	8.68	24	12	0.30	2.3
2	Ma	97.5	48.1	276	58	10	0.34	7.6
4	Villa	66.0	22.0	–	55	10	0.34	20
3	This work	2.36	2.09	–	47	10	0.33	3.1
3	This work	1.92	1.80	–	20	6	0.23	1.7

Table 6

Cross-correlation matrix between the constants of the 6-parameter kinetic model. The overall cross-correlation is low, except for the Arrhenius constants.

	$k_{CO_2 A}$	$k_{RWGS A}$	$k_{CO_2 B}$	$k_{RWGS B}$	$k_{H_2O/9}$	k_{H_2}
$k_{CO_2 A}$	1.00	0.25	1.00	0.26	0.08	0.07
$k_{RWGS A}$		1.00	0.25	1.00	-0.14	0.29
$k_{CO_2 B}$			1.00	0.26	0.02	0.05
$k_{RWGS B}$				1.00	-0.18	0.28
$k_{H_2O/9}$					1.00	0.06
k_{H_2}						1.00

fit all parameters of the 10-parameter individually. Suggested is to measure or collect a dataset with low molar hydrogen concentrations, varying partial pressures and incorporating experiments with methanol and/or water in the reactor feed.

From Fig. 6 the differences between the models become clear. BF is not able to predict the CO₂ conversion at pressures higher than 30 bar, and shows a constant conversion level, which is not expected based on literature findings [46]. The newly proposed 6 parameter kinetic model can predict both trends, with a predictive capability which is in the same range or better than the models from Graaf and Seidel. The selectivity below 20 bar in Fig. 6 lies above the equilibrium-based selectivity for all models. It can either be that the constants of the model are wrong or that this is actually a kinetic effect. This could be very interesting to experimentally investigate this aspect further.

Fig. 7 and 8 show that BF and Graaf exhibit some deviating behavior in a CSTR reactor, with a pure CO feed, a pressure of 70 bar and a different catalyst manufacturer. The conversion and selectivity are respectively defined as in Eq. (55) and (56). BF and Graaf come close in absolutely predicting the data points, but are strongly deviating outside the domain. On the other hand it is remarkable that the models of this work and Seidel seem to correctly predict this behavior, despite the fact that this is on the complete other side of the spectrum. It is hard to tell from these data points whether the proposed model or Seidel is predicting better outside these domains, however more experiments could provide answers.

$$\zeta_{CO} = 1 - \frac{y_{CO,out} \gamma}{y_{CO,in}} \quad (55)$$

$$\sigma_{MeOH} = 1 - \frac{y_{CO_2,out} \gamma}{y_{CO,in} - y_{CO,out} \gamma} \quad (56)$$

5.3. Fugacities

The fugacities were calculated for each experiment. The figure is given in the Supporting information. On average the deviation from

ideal behaviour is around 2.5 %, but at higher pressures (> 50 bar) the deviation can be more than 5 %. The components that are deviating the most from ideal behavior are H₂, methanol and water. It is difficult to measure those components precisely experimentally, so using fugacities can improve overall predictions. The most important influence on the fugacities is the total amount of methanol and water. When the total mole fraction of these condensable compounds gets above 0.1 the deviations become large and fugacities must be taken into account. Overall, one can argue to use ideal gas assumptions up to 50 bar, as long as the total mole fraction of methanol and water stays below 0.1.

5.4. Influence of catalyst preparation method

One of main results is also that two different Cu/ZnO/Al₂O₃ catalysts were able to be regressed together in a combined dataset. Since the regressed models succeeded in predicting both, it can be stated that the method of preparing (for these catalysts) is of very little influence. This is shown in Figs. 5 and 7. The prediction of the absolute values of CO conversion in a different reactor with a different catalyst is close to the experimental value. The prediction of data is, as can be seen most distinctively in Fig. 7, much more dependent on the type of model. It also depends much more on the size of the original dataset on which the model was regressed. Proof of that is the fact that the original model of Seidel et al. was perfectly predicting their dataset, but not the data added in this work (reflected in the value of χ^2_{orig} of Seidel et al.). After regression it is still predicting their original dataset equally well, but now it also predicts our dataset well. So, the method of preparation is negligible in the scope of this research.

6. Model selection

Selecting a good kinetic model is not easy and it cannot be done based on a single parameter. From the results in Table 5 it became clear that the Seidel model predicts the experimental data the best and one could opt for taking simply the best model. However, as was stated in the parameter estimation section, a kinetic model should follow certain rules. The fourth rule is checked and shown in Table 7. The adsorption isotherms were assumed to be constant by Seidel et al. So the validity cannot be directly checked. In that case the values from the fitted adsorption isotherms of Vanden Bussche and Froment are used to get an estimate of the validity of the fitted constants, the values can be found in the Supporting information. The same holds for the Graaf model. This check cannot be performed with the 6-parameter model, since no individual adsorption constants were fitted, just their ratios.

Based on the fourth rule only Graaf, BF and the 10-parameter model are valid. Since the 10-parameter model is physically correct, it is likely that this also holds for the 6-parameter model. In statistics there is a simple rule for when to decide among different models. The rule is:

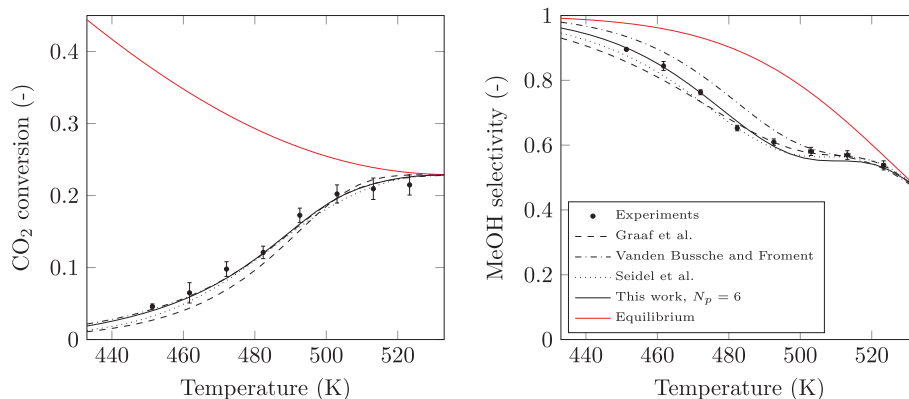


Fig. 5. On the left: CO₂ conversion over temperature curve. On the right: Methanol selectivity based on the CO measurements over temperature curve. Experiments of group 2, P = 40 bara, $\phi_V = 100 \text{ mL min}^{-1}/\text{GHSV} = 3000 \text{ h}^{-1}$, CO₂/H₂ = 25/75%_{mole}.

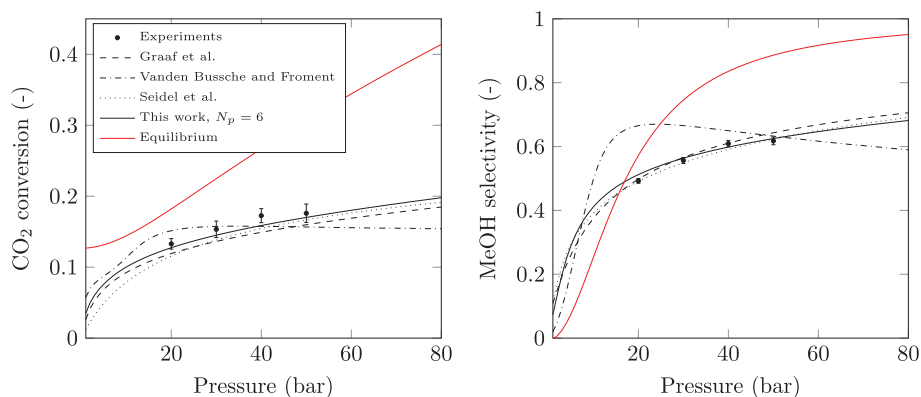


Fig. 6. On the left: CO₂ conversion over pressure curve. On the right: Methanol selectivity based on the CO measurements over pressure curve. Experiments of group 2, T = 493 K, $\phi_V^\circ = 100 \text{ mL min}^{-1}/\text{GHSV} = 3000 \text{ h}^{-1}$, CO₂/H₂ = 25/75%_{mole}.

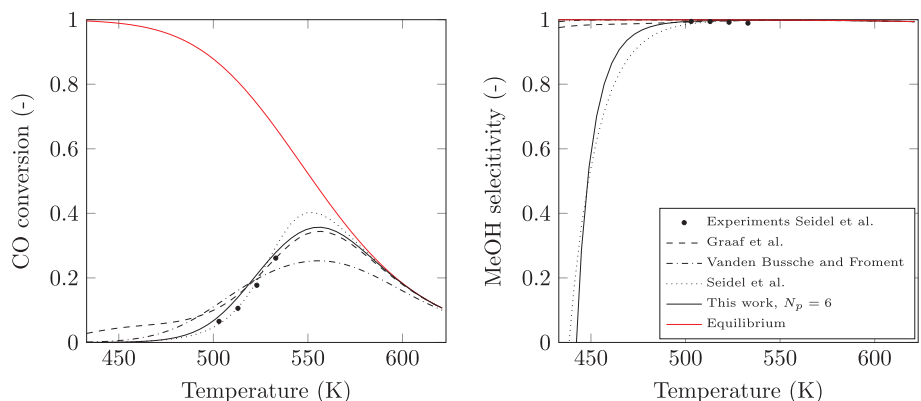


Fig. 7. On the left: CO conversion over temperature curve. On the right: Methanol selectivity based on the CO₂ measurements over temperature curve. Experiments of Seidel et al. [20], P = 70 bara, $\phi_V^\circ = 238 \text{ mL min}^{-1}/\text{GHSV} = 4000 \text{ h}^{-1}$, CO/H₂/N₂ = 11.34/72.91/15.74%_{mole}.

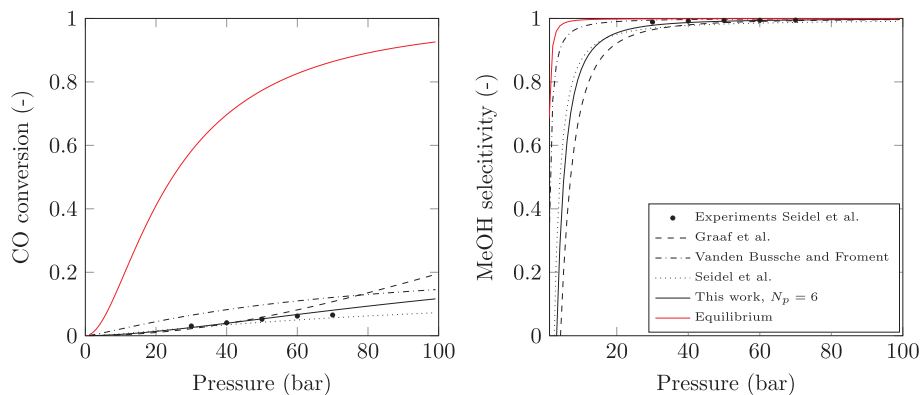


Fig. 8. On the left: CO conversion over pressure curve. On the right: Methanol selectivity based on the CO₂ measurements over pressure curve. Experiments of Seidel et al. [20], T = 503 K, $\phi_V^\circ = 238 \text{ mL min}^{-1}/\text{GHSV} = 4000 \text{ h}^{-1}$, CO/H₂/N₂ = 11.34/72.91/15.74%_{mole}.

choose the model with the least number of parameters, that is still able to predict the experimental data within one standard deviation. To check this the following calculation is introduced:

$$\hat{w}_{pred} = \frac{1}{N} \frac{1}{N_c} \sum_{i=1}^N \sum_{j=1}^{N_c} (w_i - \sigma_{w_i}) < \hat{w}_i < (w_i + \sigma_{w_i}) \quad (57)$$

The relation indicates what the percentage of correctly predicted points is within one standard deviation. The results are shown in Table 7. From the \hat{w}_{pred} value it becomes clear that the 6-parameter model is almost as good as the model of Seidel. The difference is only 5% for half the amount of parameters. Based on the good fit (χ^2_{best}), the good predictive properties ($CV_{(5)}$), as well as Gaikwad et al. [46], the

low variance $\sigma_{p,avg}$, the low cross-correlation (Table 6) and the statistically good prediction (\hat{w}_{pred}), the six parameter model is selected as the best model.

6.1. Selected kinetic model

The fitted parameters for the 6-parameter model are shown in Table 8, the rest of the fitted parameters for each model can be found in the Supporting information. The relatively large activation energies are a result of the lumping procedure of the adsorption isotherms. The pre-exponential factor must increase to compensate for this. The errors shown are the standard deviations of the parameters over the five fits as produced with the cross-validation method. The error is quite large in

Table 7

Physical feasibility check of $-\Delta S_{ads}^{\circ}$ (J/molK) of all of the kinetic models. The value shown should not exceed the S_{gas}° as shown in the last column [51]. Values with an asterisk (*) are estimated values, since they were not directly fitted.

	Graaf	BF	Seidel	Ma	Villa	$N_p = 10$	$N_p = 6$	S_{gas}° (J/molK)
CO ₂	143	–	452*	233	163	–	–	< 214
CO	125	–	25*	166	229	–	–	< 198
H ₂	32*	5.7	32*	466	140	15	–	< 131
CH ₃ OH	–	–	–	–	–	62	–	< 240
H ₂ O	130*	130	316*	–	–	–	–	< 189
\hat{w}_{pred} (%)	51	50	63	32	38	58	58	

Table 8

Estimated values of the 6-parameter model as proposed in this work. The corresponding equations can be found in eqs. (40), (41) and (52). The significant numbers shown are needed to keep the same quality of the original fit. The shown error is the standard deviation over the five fits as produced with the cross-validation method. The parameters of the other models can be found in the Supporting information.

Parameter		Estimated value	
$\ln(k_{CO_2})$	a	34.24 ± 0.71	$k_{CO_2} = 7.414 \cdot 10^{14} \exp\left(\frac{-166,000}{RT}\right)$
	b	$19,960 \pm 180$	
$\ln(k_{RWGS})$	a	43.85 ± 1.2	$k_{RWGS} = 1.111 \cdot 10^{19} \exp\left(\frac{-203,700}{RT}\right)$
	b	$24,500 \pm 610$	
$k_{H_2O/9}$		126.4 ± 66	
k_{H_2}		1.099 ± 0.66	

the activation energy of the RWGS rate constant, so this parameter is sensitive to changes in experimental data.

The results of the model are shown in parity plots per component in Figs. 9 and 10. The parity plots show that the model predicts the data within a small deviation. The experimental error is reflected the most in methanol and water concentrations. More accurate experiments on methanol and water compositions are required to improve this prediction. It can be concluded from these parity plots that both PFR and CSTR type experiments can be predicted by a single kinetic rate model. Moreover, in the experiments of Seidel et al. a catalyst from a different manufacturer (BASF) was used. From the parity plots it seems there is little difference in the quality of the prediction, since no clear shift in

data can be seen. Thus the model seems to be valid for industrial methanol catalysts of more than one manufacturer. The conditions applied during the experiments for which the model is regressed and tested are common industrial operating conditions. It is therefore expected that the novel model will perform well in modeling industrial plants and reactors. In very specific domains (like very low pressures or hydrogen concentrations), which are far outside the datasets used for regression, somewhat larger deviations may occur.

7. Conclusion

In this work a comparison is made between the kinetic models of Graaf et al., Vanden Bussche and Froment, Seidel et al., Ma et al. and Villa et al. by refitting the kinetic models on the same dataset of 234 experiments, measured in two different facilities. The regression method allowed for a good insight into the model predictive capabilities and variance. It is shown that a single kinetic model can be used for both PFR- and CSTR-type reactors. It is also shown that current industrial catalysts from different manufacturers can be predicted with a single model. The model regression is done using fugacities. However, ideal gas law behaviour may be considered, as long as the total mole fraction of methanol and water does not exceed 0.1 and/or the pressure is not higher than 50 bar. The models of Ma et al. and Villa et al. are not suitable. Graaf et al. is partially physically valid and fitting well, but does not perform well in predicting outside the training set. The Vanden Bussche and Froment model is physically sound, but also not performing well in predicting outside the original dataset. The model of Seidel et al. could predict the data the best in terms of a mean squared error analysis, but is complex and has highly correlated parameters.

A new kinetic model, on the basis of the Vanden Bussche and Froment model is derived and adapted to fully comply with recent literature findings of catalyst behavior. Screening of rate determining steps turned out to be quite powerful with only six parameters. The result is that $HCOOH \rightleftharpoons HCO + OH$ has the best match, although it is still a statistically insignificant difference compared with the well-known formate hydrogenation. So, more discriminating experiments are needed to substantiate this.

The six parameter model can predict the trends in the experimental data very well, with the same order of magnitude of deviation as regressed models with many more parameters. Therefore, the six parameter model is one that is statistically valid with the current dataset and expected to change little in parameter values (around 20%) when new data is added. It is a good predicting model, as confirmed by the cross-validation method and an external data set. The entire dataset

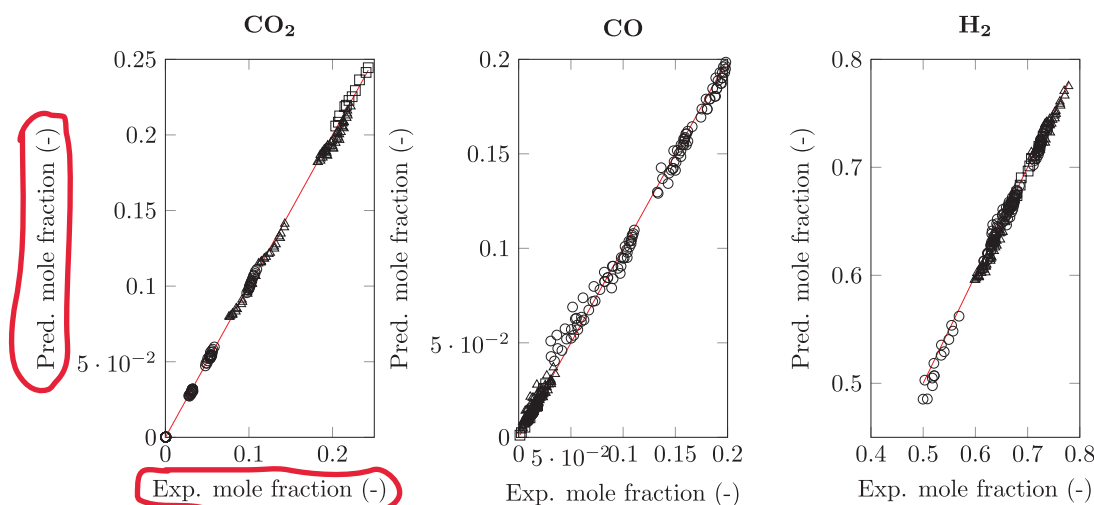


Fig. 9. Parity plot of the proposed 6-parameter model for components CO₂, CO and H₂. The circles (○) represent the data of Seidel et al. [20], the triangles (Δ) the data of group 2 and the squares (□) the data of group 1. The dataset has a total of 234 experiments. The red line is the parity line.

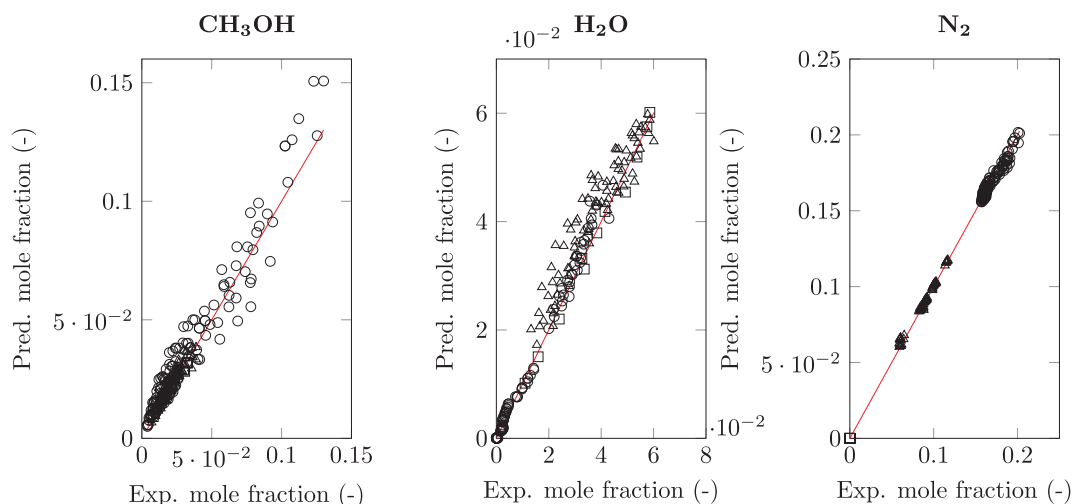


Fig. 10. Parity plot of the proposed 6-parameter model for components methanol, water and N₂. The circles (○) represent the data of Seidel et al. [20], the triangles (Δ) the data of group 2 and the squares (□) the data of group 1. The dataset has a total of 234 experiments. The red line is the parity line.

Table 9

Summary of all equations and variables needed for the 6-parameter methanol kinetics model. The fugacity (f_i) has the unit bar and r_i has the unit mol/kg_{cat}s.

Equation or variable	Ref.
$r_{CO_2} = k_{CO_2} f_{CO_2} f_{H_2}^2 \left(1 - \frac{1}{K_{PCO_2}(T)} \frac{f_{CH_3OH} f_{H_2O}}{f_{H_2}^3 f_{CO_2}} \right) \theta^*$	Eq. (52)
$r_{RWGS} = k_{RWGS} f_{CO_2} f_{H_2}^{\frac{1}{2}} \left(1 - \frac{1}{K_{PRWGS}(T)} \frac{f_{CO} f_{H_2O}}{f_{CO_2} f_{H_2}} \right) \theta^*$	Eq. (40)
$\theta^* = \left(f_{H_2}^{\frac{1}{2}} k_{H_2} + f_{H_2O} k_{H_2O/9} + f_{CH_3OH} \right)^{-1}$	Eq. (41)
$k_{CO_2} = 7.414 \cdot 10^{14} \exp\left(\frac{-166,000}{RT}\right)$	Table 8
$k_{RWGS} = 1.111 \cdot 10^{19} \exp\left(\frac{-203,700}{RT}\right)$	Table 8
$k_{H_2O/9} = 126.4$	Table 8
$k_{H_2} = 1.099$	Table 8
$K_{PCO_2}(T) = K_{PCO}(T) K_{PRWGS}(T)$	Ref. [32]
$K_{PRWGS}(T)$	Ref. [32]

covers most industrial domains, making the six parameter well suited for modeling applications of reactors or flow-sheets. It is suggested to use the newly proposed six parameter model for steady state calculations of methanol synthesis. A summary of the equations of the proposed model together with the estimated variables and references is given in Table 9.

Declaration of Competing Interest

The authors declare that they have no known competing financial interests or personal relationships that could have appeared to influence the work reported in this paper.

Acknowledgments

We thank the National Institute of Chemistry of Slovenia, the Kemijski inštitut for hosting part of the research. Thanks to the supervisors Neja Strah Štefanič and Anže Prašnikar and the methanol reactor engineer Matic Grom. Also thanks to Dr. Uroš Novak for several analysis of the produced liquid phase. We also thank for the valuable input of Jimmy Faria Albanese from the University of Twente by proof

reading the article. We also thank Sjors de Groot for validating the kinetic equations and Tim van Schagen for validating the kinetic model. The authors declare no competing interest. This research did not receive any specific grant from funding agencies in the public, commercial, or not-for-profit sectors.

Appendix A. Supplementary data

Supplementary data associated with this article can be found, in the online version, at <https://doi.org/10.1016/j.cej.2020.124181>.

References

- [1] M.J. Bos, D.W.F. Brilman, A novel condensation reactor for efficient CO₂ to methanol conversion for storage of renewable electric energy, *Chem. Eng. J.* 278 (2015) 527–532, <https://doi.org/10.1016/J.CEJ.2014.10.059>.
- [2] G.A. Olah, Towards oil independence through renewable methanol chemistry, *Angew. Chem. Int. Ed.* 52 (1) (2013) 104–107, <https://doi.org/10.1002/anie.201204995>.
- [3] S.G. Jadhav, P.D. Vaidya, B.M. Bhanage, J.B. Joshi, Catalytic carbon dioxide hydrogenation to methanol: a review of recent studies, *Chem. Eng. Res. Des.* 92 (11) (2014) 2557–2567, <https://doi.org/10.1016/J.CHERD.2014.03.005>.
- [4] A. Alarifi, A. Elkamel, E. Croiset, Steady-state simulation of a novel annular multitubular reactor for enhanced methanol production, *Ind. Eng. Chem. Res.* 52 (44) (2013) 15387–15393, <https://doi.org/10.1021/ie4006589>.
- [5] T. Blumberg, T. Morosuk, G. Tsatsaronis, Exergy-based evaluation of methanol production from natural gas with CO₂ utilization, *Energy* 141 (2017) 2528–2539, <https://doi.org/10.1016/j.energy.2017.06.140>.
- [6] S. Szima, C.C. Cormos, Improving methanol synthesis from carbon-free H₂ and captured CO₂: a techno-economic and environmental evaluation, *J. CO₂ Util.* 24 (2018) 555–563, <https://doi.org/10.1016/j.jcou.2018.02.007>.
- [7] M. Asif, X. Gao, H. Lv, X. Xi, P. Dong, Catalytic hydrogenation of CO₂ from 600 MW supercritical coal power plant to produce methanol: a techno-economic analysis, *Int. J. Hydrogen Energy* 43 (5) (2018) 2726–2741, <https://doi.org/10.1016/j.ijhydene.2017.12.086>.
- [8] M. Kaiser, H. Freund, A multimodular pseudoheterogeneous model framework for optimal design of catalytic reactors exemplified by methanol synthesis, *Chem. Eng. Sci.* 206 (2019) 401–423, <https://doi.org/10.1016/J.CES.2019.04.036>.
- [9] B. Rahmatmand, M.R. Rahimpour, P. Keshavarz, Introducing a novel process to enhance the syngas conversion to methanol over Cu/ZnO/Al₂O₃ catalyst, *Fuel Process. Technol.* 193 (2019) 159–179, <https://doi.org/10.1016/J.FUPROC.2019.05.014>.
- [10] E. Moïoli, R. Mutschler, A. Züttel, Renewable energy storage via CO₂ and H₂ conversion to methane and methanol: assessment for small scale applications, *Renew. Sustain. Energy Rev.* 107 (2019) 497–506, <https://doi.org/10.1016/J.RSER.2019.03.022>.
- [11] M.J. Bos, Y. Slotboom, S.R.A. Kersten, D.W.F. Brilman, Characterization of a condensing CO₂ to methanol reactor, *Ind. Eng. Chem. Res.* <https://doi.org/10.1021/acs.iecr.9b02576>.
- [12] J.J. Meyer, P. Tan, A. Apfelbacher, R. Daschner, A. Hornung, Modeling of a methanol synthesis reactor for storage of renewable energy and conversion of CO₂ – comparison of two kinetic models, *Chem. Eng. Technol.* 39 (2) (2016) 233–245, <https://doi.org/10.1002/ceat.201500084>.
- [13] P. Villa, P. Forzatti, G. Buzzi-Ferraris, G. Garone, I. Pasquon, Synthesis of alcohols

¹ Assuming a volume of 3.6 mL.

- from carbon oxides and hydrogen. 1. Kinetics of the low-pressure methanol synthesis, *Ind. Eng. Chem. Process Des. Develop.* 24 (1) (1985) 12–19, <https://doi.org/10.1021/i200028a003>.
- [14] J. Skrzypek, M. Lachowska, H. Moroz, Kinetics of methanol synthesis over commercial copper/zinc oxide/alumina catalysts, *Chem. Eng. Sci.* 46 (11) (1991) 2809–2813, [https://doi.org/10.1016/0009-2509\(91\)85150-V](https://doi.org/10.1016/0009-2509(91)85150-V).
- [15] T.S. Askgaard, J.K. Nørskov, C.V. Ovesen, P. Stoltze, A kinetic model of methanol synthesis, *J. Catal.* 156 (2) (1995) 229–242, <https://doi.org/10.1006/jcat.1995.1250>.
- [16] K.M. Vanden Bussche, G.F. Froment, A steady-state kinetic model for methanol synthesis and the water gas shift reaction on a commercial Cu/ZnO/Al₂O₃ catalyst, *J. Catal.* 161 (1) (1996) 1–10, <https://doi.org/10.1006/jcat.1996.0156>.
- [17] T. Kubota, I. Hayakawa, H. Mabuse, K. Mori, K. Ushikoshi, T. Watanabe, M. Saito, Kinetic study of methanol synthesis from carbon dioxide and hydrogen, *Appl. Organomet. Chem.* 15 (2) (2001) 121–126, [https://doi.org/10.1002/1099-0739\(200102\)15:2<121::AID-AOC106>3.0.CO;2-3](https://doi.org/10.1002/1099-0739(200102)15:2<121::AID-AOC106>3.0.CO;2-3).
- [18] G. Liu, D. Willcox, M. Garland, H.H. Kung, The role of CO₂ in methanol synthesis on CuZn oxide: an isotope labeling study, *J. Catal.* 96 (1) (1985) 251–260, [https://doi.org/10.1016/0021-9517\(85\)90378-1](https://doi.org/10.1016/0021-9517(85)90378-1).
- [19] G.H. Graaf, E.J. Stamhuis, A.A.C.M. Beenackers, Kinetics of low-pressure methanol synthesis, *Chem. Eng. Sci.* 43 (12) (1988) 3185–3195, [https://doi.org/10.1016/0009-2509\(88\)85127-3](https://doi.org/10.1016/0009-2509(88)85127-3).
- [20] C. Seidel, A. Jörke, B. Vollbrecht, A. Seidel-Morgenstern, A. Kienle, Kinetic modeling of methanol synthesis from renewable resources, *Chem. Eng. Sci.* 175 (2018) 130–138, <https://doi.org/10.1016/j.ces.2017.09.043>.
- [21] M.A. McNeil, C.J. Schack, R.G. Rinker, Methanol synthesis from hydrogen, carbon monoxide and carbon dioxide over a CuO/ZnO/Al₂O₃ catalyst: II. Development of a phenomenological rate expression, *Appl. Catal.* 50 (1) (1989) 265–285, [https://doi.org/10.1016/S0166-9834\(00\)80841-6](https://doi.org/10.1016/S0166-9834(00)80841-6).
- [22] T. Henkel, Modellierung von Reaktion und Stofftransport in geformten Katalysatoren am Beispiel der Methanolsynthese, Ph.D. thesis (2011). URL:<https://mediatum.ub.tum.de/doc/1080247/1080247.pdf>.
- [23] M. Takagawa, M. Ohsugi, Study on reaction rates for methanol synthesis from carbon monoxide, carbon dioxide, and hydrogen, *J. Catal.* 107 (1) (1987) 161–172, [https://doi.org/10.1016/0021-9517\(87\)90281-8](https://doi.org/10.1016/0021-9517(87)90281-8).
- [24] K. Klier, V. Chatikavanij, R.G. Herman, G.W. Simmons, Catalytic synthesis of methanol from CO/H₂: IV. The effects of carbon dioxide, *J. Catal.* 74 (2) (1982) 343–360, [https://doi.org/10.1016/0021-9517\(82\)90040-9](https://doi.org/10.1016/0021-9517(82)90040-9).
- [25] H. Ma, W. Ying, D. Fang, Study on methanol synthesis from coal-based syngas, *J. Coal Sci. Eng. (China)* 15 (1) (2009) 98–103, <https://doi.org/10.1007/s12404-009-0120-y>.
- [26] B.S. Clausen, J. Schiøtz, L. Grabæk, C.V. Ovesen, K.W. Jacobsen, J.K. Nørskov, H. Topsøe, Wetting/ non-wetting phenomena during catalysis: Evidence from in situ on-line EXAFS studies of Cu-based catalysts, *Top. Catal.* 1 (3–4) (1994) 367–376, <https://doi.org/10.1007/BF01492289>.
- [27] M. Muhler, E. Tornqvist, L.P. Nielsen, B.S. Clausen, H. Topsøe, On the role of adsorbed atomic oxygen and CO₂ in copper-based methanol synthesis catalysts, *Catal. Lett.* 25 (1–2) (1994) 1–10, <https://doi.org/10.1007/bf00815409>.
- [28] Y. Choi, K. Futagami, T. Fujitani, J. Nakamura, The difference in the active sites for CO₂ and CO hydrogenations on Cu/ZnO-based methanol synthesis catalysts, *Catal. Lett.* 73 (1) (2001) 27–31, <https://doi.org/10.1023/A:1009074219286>.
- [29] E.L. Kunkes, F. Studt, F. Abild-Pedersen, R. Schlögl, M. Behrens, Hydrogenation of CO₂ to methanol and CO on Cu/ZnO/Al₂O₃: is there a common intermediate or not? *J. Catal.* 328 (2015) 43–48, <https://doi.org/10.1016/j.jcat.2014.12.016>.
- [30] T. Kandemir, M. Friedrich, S.F. Parker, F. Studt, D. Lennon, R. Schlögl, M. Behrens, Different routes to methanol: inelastic neutron scattering spectroscopy of adsorbates on supported copper catalysts, *Phys. Chem. Chem. Phys.* 18 (26) (2016) 17253–17258, <https://doi.org/10.1039/c6cp00967k>.
- [31] N. Park, M.-J. Park, Y.-J. Lee, K.-S. Ha, K.-W. Jun, Kinetic modeling of methanol synthesis over commercial catalysts based on three-site adsorption, *Fuel Process. Technol.* 125 (2014) 139–147, <https://doi.org/10.1016/J.FUPROC.2014.03.041>.
- [32] G.H. Graaf, J.G.M. Winkelman, Chemical equilibria in methanol synthesis including the water-gas shift reaction: a critical reassessment, *Ind. Eng. Chem. Res.* 55 (20) (2016) 5854–5864, <https://doi.org/10.1021/acs.iecr.6b00815>.
- [33] J.G. Van Bennekom, J.G. Winkelman, R.H. Venderbosch, S.D. Nieland, H.J. Heeres, Modeling and experimental studies on phase and chemical equilibria in high-pressure methanol synthesis, *Ind. Eng. Chem. Res.* 51 (38) (2012) 12233–12243, <https://doi.org/10.1021/ie3017362>.
- [34] M. Schwaab, L.P. Lemos, J.C. Pinto, Optimum reference temperature for reparameterization of the Arrhenius equation. Part 2: problems involving multiple reparameterizations, *Chem. Eng. Sci.* 63 (11) (2008) 2895–2906, <https://doi.org/10.1016/j.ces.2008.03.010>.
- [35] C.V. Ovesen, B.S. Clausen, J. Schiøtz, P. Stoltze, H. Topsøe, J.K. Nørskov, Kinetic implications of dynamical changes in catalyst morphology during methanol synthesis over Cu/ZnO catalysts, *J. Catal.* 168 (2) (1997) 133–142, <https://doi.org/10.1006/JCAT.1997.1629>.
- [36] K.J. Smith, Synthesis of alcohols from carbon oxides and hydrogen. 1. Kinetics of the low-pressure methanol synthesis, *Comments Ind. Eng. Chem. Res.* 26 (2) (1987) 400–401, <https://doi.org/10.1021/ie00062a042>.
- [37] L.C. Grabow, M. Mavrikakis, Mechanism of methanol synthesis on Cu through CO₂ and CO hydrogenation, *ACS Catal.* 1 (4) (2011) 365–384, <https://doi.org/10.1021/cs200055d>.
- [38] H.W. Lim, M.J. Park, S.H. Kang, H.J. Chae, J.W. Bae, K.W. Jun, Modeling of the kinetics for methanol synthesis using Cu, *Ind. Eng. Chem. Res.* 48 (23) (2009) 10448–10455.
- [39] V.D.B.C. Dasireddy, N. Strah, B. Likozar, Correlation between synthesis pH, structure and Cu/MgO/Al₂O₃ heterogeneous catalyst activity and selectivity in CO₂ hydrogenation to methanol, *J. CO₂ Util.* 28 (2018) 189–199, <https://doi.org/10.1016/j.jcou.2018.09.002>.
- [40] V.D.B.C. Dasireddy, N. Strah, M. Hu, B. Likozar, Effect of alkaline earth metal oxide (MO) Cu/MO/Al₂O₃ catalysts on methanol synthesis activity and selectivity via CO₂ reduction, *Fuel* 233 (2018) 103–112, <https://doi.org/10.1016/j.fuel.2018.06.046>.
- [41] F. Manenti, S. Cieri, M. Restelli, Considerations on the steady-state modeling of methanol synthesis fixed-bed reactor, *Chem. Eng. Sci.* 66 (2) (2011) 152–162, <https://doi.org/10.1016/j.ces.2010.09.036>.
- [42] P.B. Weisz, C.D. Prater, Interpretation of Measurements in Experimental Catalysis vol. 6, Academic Press, 1954, pp. 143–196 doi:[https://doi.org/10.1016/S0360-0564\(08\)60390-9](https://doi.org/10.1016/S0360-0564(08)60390-9).
- [43] D.E. Mears, Tests for transport limitations in experimental catalytic reactors, *Ind. Eng. Chem. Process Des. Develop.* 10 (4) (1971) 541–547, <https://doi.org/10.1021/i260040a020>.
- [44] M. Vannice, S. Hyun, B. Kalpakci, W. Liauh, Entropies of adsorption in heterogeneous catalytic reactions, *J. Catal.* 56 (3) (1979) 358–362, [https://doi.org/10.1016/0021-9517\(79\)90128-3](https://doi.org/10.1016/0021-9517(79)90128-3).
- [45] G. James, D. Witten, T. Hastie, R. Tibshirani, An Introduction to Statistical Learning: with Applications in R, Springer Texts in Statistics, Springer, New York, 2013.
- [46] R. Gaikwad, A. Bansode, A. Urakawa, High-pressure advantages in stoichiometric hydrogenation of carbon dioxide to methanol, *J. Catal.* 343 (2016) 127–132, <https://doi.org/10.1016/J.JCAT.2016.02.005>.
- [47] K. Kobl, S. Thomas, Y. Zimmermann, K. Parkhomenko, A.-C. Roger, Power-law kinetics of methanol synthesis from carbon dioxide and hydrogen on copper-zinc oxide catalysts with alumina or zirconia supports, *Catal. Today* 270 (2016) 31–42, <https://doi.org/10.1016/J.CATTOD.2015.11.020>.
- [48] Y.-F. Zhao, Y. Yang, C. Mims, C.H. Peden, J. Li, D. Mei, Insight into methanol synthesis from CO₂ hydrogenation on Cu(111): Complex reaction network and the effects of H₂O, *J. Catal.* 281 (2) (2011) 199–211, <https://doi.org/10.1016/j.jcat.2011.04.012>.
- [49] Y. Yang, C. Mims, D. Mei, C. Peden, C. Campbell, Mechanistic studies of methanol synthesis over Cu from CO/CO₂/H₂/H₂O mixtures: the source of C in methanol and the role of water, *J. Catal.* 298 (2013) 10–17, <https://doi.org/10.1016/J.JCAT.2012.10.028>.
- [50] J.B. Hansen, The methanol synthesis past and future (Tech. rep.), Haldor Topsøe, 2017 URL:https://brintbranchen.dk/wp-content/uploads/2017/10/John-Boegild-Hansen_Topsøe.pdf.
- [51] W.M. Haynes, D.R. Lide, T.J. Bruno, CRC handbook of chemistry and physics: a ready-reference book of chemical and physical data, 2016th ed., CRC Press, Boca Raton, Florida, 2017 URL:<http://hbcponline.com>.